Article

The International Journal of Robotics Research
1–25
© The Author(s) 2020
Article reuse guidelines:
sagepub.com/journals-permissions
DOI: 10.1177/0278364920961452
journals.sagepub.com/home/ijr
SAGE

A hip–knee–ankle exoskeleton emulator for studying gait assistance

Gwendolyn M Bryan[1,2*], Patrick W Franks[1,2*], Stefan C Klein[1,2], Robert J Peuchen[3] and Steven H Collins[1,2]

Abstract

Lower-limb exoskeletons could improve the mobility of people with disabilities, older adults, workers, first responders, and military personnel. Despite recent advances, few products are commercially available and exoskeleton research is still often limited by hardware constraints. Many promising multi-joint assistance strategies, especially those with high-torque and high-power components, have yet to be tested because they are beyond the capabilities of current devices. To study these untested assistance strategies, we present a hip–knee–ankle exoskeleton emulator that can apply high torques and powers that match or exceed those observed in uphill running. The system has powerful off-board motors that actuate a 13.5 kg exoskeleton end effector worn by the user. It can apply up to 200 Nm of torque in hip flexion, hip extension, and ankle plantarflexion, 250 Nm of torque in knee extension, and 140 Nm of torque in knee flexion, with over 4.5 kW of power at each joint and a closed-loop torque bandwidth of at least 18 Hz in each direction of actuation. The exoskeleton is compliant in unactuated directions, adjustable for a wide range of users and comfortable during walking and running. When paired with human-in-the-loop optimization, we expect that this system will identify new assistance strategies to improve human mobility. A complete computer-aided design (CAD) model of the exoskeleton and a bill of materials are included and available for download.

Keywords

Exoskeleton design, human augmentation, locomotion, wearable robotics

1. Introduction

Lower-limb exoskeletons have the potential to improve a person's ability to walk, run, jump, and carry loads by applying assistive joint torques. They could improve assistance for people with disabilities and older adults and could increase the performance of workers, first responders and military personnel. Currently, exoskeletons are in a nascent stage of development with few products on the market (Sawicki et al., 2020; Yan et al., 2015; Young and Ferris, 2017). Some exoskeletons have focused on walking assistance or rehabilitation for people with impairments (Baunsgaard et al., 2018; Esquenazi et al., 2012; Farris et al., 2011; Griffin et al., 2017; Jezernik et al., 2003; Jin et al., 2015; Kilicarslan et al., 2013; Maeshima et al., 2011; Wang et al., 2015), while another group of devices have focused on performance augmentation for walking and running.

Some performance-augmenting exoskeletons have already shown improvements to locomotor performance, usually measured as reductions in metabolic cost relative to the device turned off (Young and Ferris, 2017). Of the exoskeletons that have shown improvements during walking, most have assisted either the ankles (Awad et al., 2017; Collins et al., 2015; Malcolm et al., 2013; Mooney et al., 2014; Sawicki and Ferris, 2008; Zhang et al., 2017) or the hips (Ding et al., 2018; Seo et al., 2016; Young et al., 2017a). A few multi-joint exoskeletons have also reduced the metabolic cost of walking by assisting either the hips and ankles (Lee et al., 2018; Quinlivan et al., 2017) or the knees and ankles (Malcolm et al., 2018a). While most of these effective exoskeletons are tethered, some of them are mobile (Collins et al., 2015; Kim et al., 2019; Lee et al., 2018; Mooney et al., 2014; Seo et al.,

[1]Mechanical Engineering, Stanford University, USA
[2]Mechanical Engineering, Carnegie Mellon University, USA
[3]BioMechanical Engineering, Delft University of Technology, Netherlands

*These authors contributed equally to this work, their names are in alphabetical order.

Corresponding author:
Steven Collins, Mechanical Engineering, Stanford University, 450 Escondido Mall, Stanford, CA 94305, USA.
Email: stevecollins@stanford.edu

2016). In addition to walking, some exoskeletons have assisted running (Lee et al., 2017b; Nasiri et al., 2018; Simpson et al., 2019; Witte et al., 2020) and load carriage (Ding et al., 2016; Lee et al., 2018; Mooney et al., 2014). While this progress hints at the potential of exoskeleton assistance, simulations suggest that even greater metabolic cost reductions may be possible with assistance strategies that have yet to be tested (Dembia et al., 2017; Uchida et al., 2016).

Emulators are flexible research devices that can be used to quickly assess a wide range of assistance strategies for exoskeletons and prostheses (Caputo and Collins, 2014). Emulators are laboratory-bound systems that utilize off-board actuators and control hardware to manipulate simple end effectors, which are worn by a user (Caputo and Collins, 2014; Witte et al., 2017, 2015). Exoskeleton end effectors can have lower mass and higher torque with quicker, less-expensive development than complex mobile exoskeletons. As emulators can utilize such powerful and versatile off-board hardware, they can test a wide variety of different device behaviors and assess their effectiveness (Zhang et al., 2017) or simulate products without expensive prototyping (Caputo et al., 2015).

The versatility of emulators makes them well-suited for human-in-the-loop optimization. Human-in-the-loop optimization is a process in which device parameters are varied in real time based on measurements of the user, such as electromyography (EMG) or metabolic rate, to optimize performance (Ding et al., 2018; Felt et al., 2015; Kim et al., 2017; Koller et al., 2016; Zhang et al., 2017). This approach is particularly effective when paired with the versatility of an emulator, which enables quick changes of assistance parameters based on user performance (Zhang et al., 2017). This strategy has proven to be more effective in reducing metabolic cost than hand tuning device parameters (Ding et al., 2018; Zhang et al., 2017). Sample-efficient optimization algorithms could be paired with this approach to search large parameter spaces, such as those expected for hip–knee–ankle exoskeletons.

Bilateral hip–knee–ankle exoskeletons could better assist walking and running than exoskeletons that actuate one or two joints. During walking and running, the hips, knees, and ankles all significantly contribute to the total biological power (Novacheck, 1998; Roberts and Belliveau, 2005; Winter, 1991), suggesting that assistance at all of these joints may result in the largest metabolic cost reductions. A hip–knee–ankle exoskeleton could be more effective at assisting bi-articular muscles than a single-joint exoskeleton. For exoskeletons with both single-joint and multi-joint configurations, it has been shown that multi-joint assistance results in greater metabolic cost reductions (Ding et al., 2017; Malcolm et al., 2018a). It has also been shown that ankle exoskeleton assistance is more effective when applied bilaterally than unilaterally (Malcolm et al., 2018b), indicating that bilateral hip–knee–ankle assistance may also be more effective. Furthermore, biomechanical simulations indicate the greatest reductions in metabolic cost during running and loaded walking are expected when assistance is applied bilaterally at the hips, knees, and ankles (Dembia et al., 2017; Uchida et al., 2016).

Broad actuation capabilities that match or exceed biological values seen in human locomotion could give greater insight into optimal assistance strategies for various tasks. Optimal assistance strategies could have high torque, frequency, velocity, or power components that are unattainable for some exoskeletons, due to either the limitations of their actuators or structures. In some studies, the greatest metabolic reductions were found at these limits, suggesting that greater improvements may be possible with greater device capabilities (Ding et al., 2018; Quinlivan et al., 2017). When optimal assistance strategies for walking have been found within a device's capabilities, the applied torques were 60–80% of the magnitude of biological torques seen in unassisted walking (Zhang et al., 2017). High-torque activities, such as running, might also have optimal assistance strategies with peak torques that are a similar percentage of biological torques. Designing for actuation capabilities that approach or exceed biological torques seen in unassisted running increases the chance of finding globally optimal assistance strategies for those activities. Designing for high bandwidth increases the precision with which these strategies are applied (Griffiths et al., 2011).

An exoskeleton should be lightweight, compliant, well-fitted, comfortable, and safe. Worn mass, especially distal mass, should be minimized to reduce the metabolic cost penalty incurred and fatigue experienced when wearing an exoskeleton (Browning et al., 2007). It should have the necessary range of motion and compliance for its intended applications. To avoid interference with natural motions, the joint velocity capabilities should exceed those observed during that activity. Furthermore, an exoskeleton should fit well and ensure good alignment of the joints of the device to the joints of the user. It should be comfortable to enable long walking or running sessions. Finally, an exoskeleton should be safe even in the event of control failure.

Here we describe the design and characterization of a hip–knee–ankle exoskeleton emulator. This is the first cable-driven exoskeleton to assist the hips, knees, and ankles. This system has the high torque, bandwidth, velocity, and power capabilities needed to explore assistance strategies that were not possible with previous exoskeletons. We conducted benchtop tests to assess its torque and bandwidth capabilities and calculated its expected power and velocity capabilities. We also tested the range of motion, compliance and comfort of the exoskeleton. Finally, we assessed the exoskeleton's ability to apply torques during walking. This system is intended to be used in conjunction with human-in-the-loop techniques to find optimal assistance profiles for human locomotion. This work could improve our understanding of exoskeleton assistance and inform the design of future products.

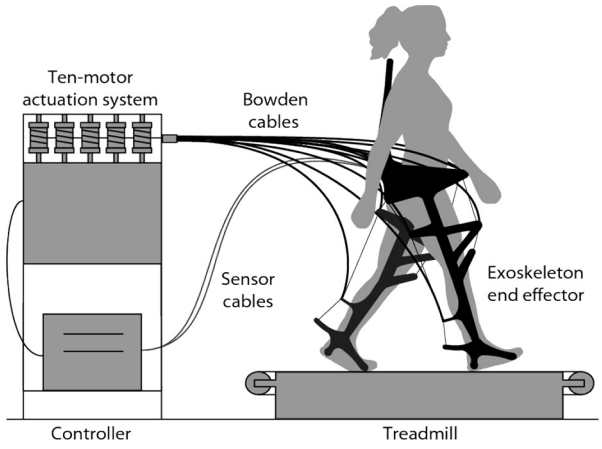

Fig. 1. Schematic of the exoskeleton emulator system. A subject wears the exoskeleton end effector while walking on a treadmill. The exoskeleton can apply torques in hip flexion, hip extension, knee flexion, knee extension, and ankle plantarflexion. The system utilizes off-board control hardware and motors, with one motor for each direction of actuation. The motor system actuates the exoskeleton end effector through a set of Bowden cable transmissions.

2. Design

We designed a hip–knee–ankle exoskeleton emulator that can apply torques in hip flexion and extension, knee flexion and extension, and ankle plantarflexion. Ten off-board motors actuate an exoskeleton end effector (Figure 1) through a set of Bowden cable transmissions. The exoskeleton can apply torques during walking at different speeds, grades, and loads, as well as during running (Multimedia extensions 1 and 2).

2.1. Exoskeleton design

The exoskeleton (Figure 2) was designed to apply large torques while minimizing worn mass. It is composed of torso, thigh, shank, and foot segments that are connected by pin joints near the user's biological joints (Figure 3). The segments are made of planar carbon fiber struts that lie on the sides of the legs and waist, and another that runs up the center of the back. These struts are lightweight, strong, and stiff in the plane in which actuation forces are applied. Owing to their geometry, they are compliant in out-of-plane bending and torsion, which allows the user to move in unactuated directions, such as hip adduction and abduction (Figure 4). Aluminum and titanium components span the width of the legs and torso to connect the struts to each other. These components experience a combination of bending and torsion and are designed with mass-efficient, hollow cross-sections. A model of the exoskeleton end effector can be found in Extension 3.

2.1.1. Torso segment. The four carbon fiber shoulder struts (Figure 5(a)) are oriented in an X-shape to run above and below the user's shoulders. Holes at the tips of these shoulder struts allow for attachment of the chest harness, and holes closer to the center of the X-shape allow for attachment of the back pad. The carbon fiber back strut (Figure 5(b)) runs down the center of the user's back and connects the shoulder struts via the back strut clamp (Figure 5(d)) to the back crossbar (Figure 5(e)). The clamps (Figure 5(c) and (d)) and back crossbar are designed for substantial torsional loads, with 50.8 mm internal clamp diameter and external tube diameter. These clamps also allow for width adjustability. The clamps and crossbar have thin walls (1.6 and 2.1 mm, respectively) for mass

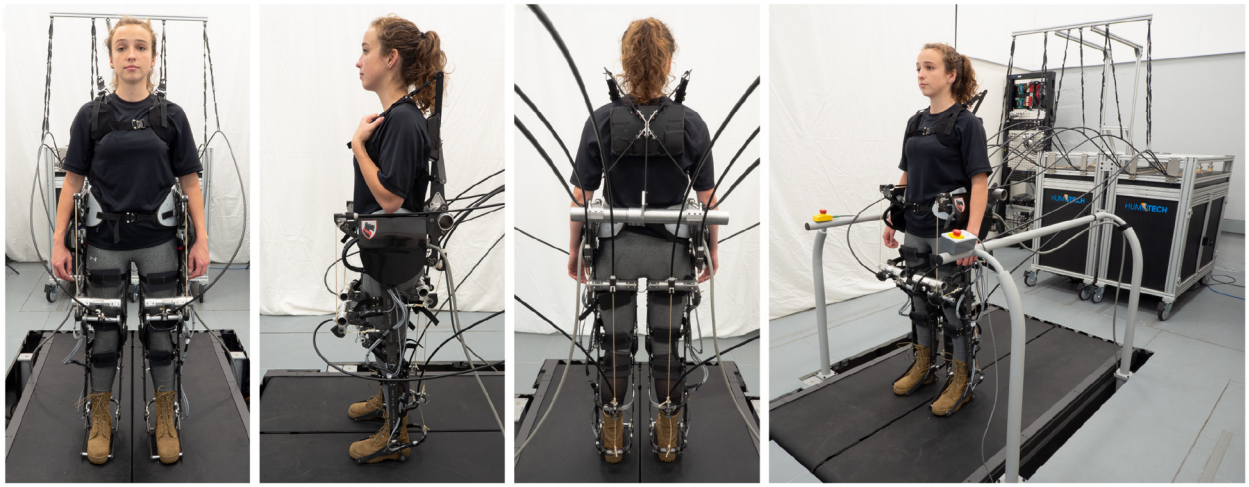

Fig. 2. User wearing the exoskeleton. (a) Front view. (b) Side view. (c) Back view. (d) Oblique view. The experimental setup includes a treadmill, 10-motor actuation system, and real-time controller. The Bowden cables are partially suspended by rubber bands to simplify cable management and reduce weight on the user.

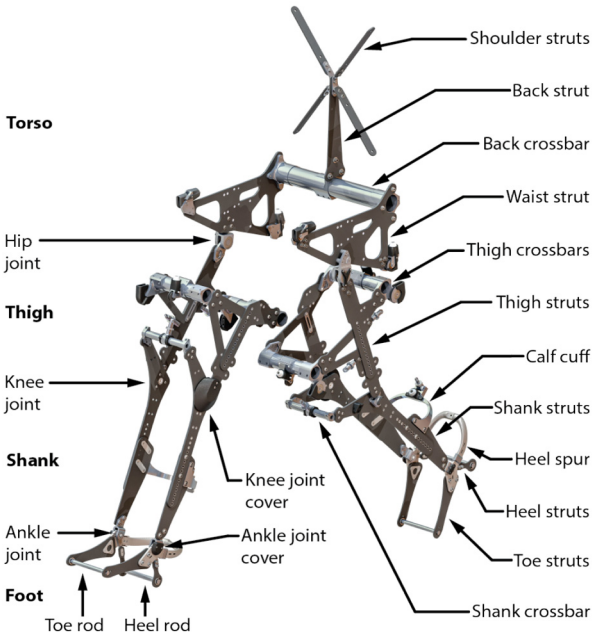

Fig. 3. Schematic of the exoskeleton end effector. The end effector is composed of planar carbon fiber struts that lie along the medial and lateral sides of the legs, sides of the waist, and the center of the back. Metal components span the legs and torso and connect the carbon fiber struts to each other. Pin joints lie close to the user's biological joints to enable motion in the sagittal plane, while compliance in the carbon fiber components allows for motion in the other directions.

efficiency and effective clamping. The carbon fiber waist struts (Figure 5(f)) lie laterally on the user's midsection. They are slightly thicker (4.7 mm) than other strut components on the exoskeleton to prevent buckling from actuation loading. Each joint assembly (Figure 5(g)) contains two ball bearings that support an axle. Their inner surfaces are nearly flush with the inner surfaces of the waist struts, so that nothing protrudes into the user's hips. An absolute magnetic encoder is fixed to the outer surface of each joint assembly by a selective-laser-sintered (SLS) nylon mount, while the magnet for the encoder is glued into the axle. The pulley assemblies (Figure 5(h)) provide termination points for the hip's outer Bowden cables and allow the inner Bowden cables to be redirected by the pulleys with minimal friction. The pulleys are made of aluminum and run on radial and thrust bushings. Each pulley axle is kept in place by external retaining rings. SLS nylon covers prevent the inner Bowden cables from falling off the pulleys and allow the attachment of elastomer (TPU) strain relief components for the outer Bowden cables. The elastomer fits inside the 3D-printed conduit attachment and encapsulates the conduit. It reduces stress concentrations on the conduit by removing the possibility of sharply bending the conduit.

2.1.2. Thigh segment. The joint assemblies (Figure 6(a) and (g)) utilize split-hub clamps to connect to the hip and knee joint axles (seen in Figures 5 and 7, respectively). The upper and lower thigh struts (Figure 6(b) and (c)) connect to each other through a series of holes to enable length adjustability of the segment. They are each connected by two bolts and threaded steel inserts (Figure 6(d)) that minimize the protrusion of fasteners into the user's leg. The hip load cell assemblies (Figure 6(e)) consist of two small threaded aluminum components, which screw onto the load cells to connect to the struts and the inner Bowden cables. SLS nylon joint covers (Figure 6(f)) bolt onto the medial knee joints to ensure any contact between the user's legs is glancing and does not result in catching. The lateral clamp and hip pulley assemblies (Figure 6(h)) redirect the inner Bowden cables for hip actuation and clamp onto the thigh

(a) (b) (c) (d)

Fig. 4. Compliance of the exoskeleton. (a) Hip abduction compliance. (b) Hip rotation compliance. (c) Spinal lateral bending compliance. (d) Spinal axial rotation compliance. The carbon fiber strut components are compliant in torsion and out of plane bending. This compliance allows users to walk and run comfortably on the treadmill.

Fig. 5. Torso segment of the exoskeleton. Assembled (left) and exploded (right) views of the torso segment of the exoskeleton. (a) Shoulder strut. (b) Back strut. (c) Lateral back crossbar clamp. (e) Medial back crossbar clamp. (e) Back crossbar. (f) Waist strut. (g) Hip joint assembly. (h) Pulley assembly.

crossbars. The pulleys run on ball bearings to ensure that the hip's inner Bowden cables are redirected towards the load cell assemblies with minimal friction to reduce cable force measurement errors. The pulleys are covered by SLS nylon components that prevent the inner cables from slipping off. The knee pulley and clamp assemblies (Figure 6(i)) provide termination points for the knee's outer Bowden cables and redirect the inner Bowden cables over nylon pulleys with ball bearings to reduce friction. The clamp assemblies (Figure 6(h), (i), and (j)) all clamp onto the thigh crossbars (Figure 6(k)). The clamps and crossbars have thin walls (1.6 and 2.1 mm, respectively) for mass efficiency and effective clamping.

2.1.3. Shank segment. The knee flexion load cell assembly (Figure 7(a)) can rotate on radial bushings on an axle mounted in the fork of the calf cuff (Figure 7(c)). The knee flexion load cell assembly is kept from rotating excessively by an SLS nylon stopper. The ankle outer Bowden cable attachment (Figure 7(b)) is composed of an SLS nylon component bolted onto the calf cuff and an elastomer (TPU) component that holds the outer Bowden cable in place. The calf cuff is bolted to the lower struts (Figure 7(k)) with custom threaded steel inserts (Figure 7(j)). The knee extension load cell assembly (Figure 7(f)) can rotate on radial bushings on the knee extension crossbar (Figure 7(d)) and is held in place laterally by SLS nylon shaft collars. The knee extension crossbar is attached to the upper shank struts (Figure 7(h)) through the knee extension clamps (Figure 7(g)). An SLS nylon hard stop (Figure 7(e)) bolts in place near the joint to prevent hyperextension and to act as strain relief for sensor cables. The knee joint assemblies (Figure 7(i)) use two ball bearings to support the knee axle. An absolute magnetic encoder is fixed to the outer surface of the lateral joint assembly by an SLS nylon mount. The encoder magnet is glued into a pocket in the axle. The upper and lower shank struts are bolted together with threaded steel inserts to provide length adjustability, similar to the thigh segment (Figure 6).

2.1.4. Foot segment. A titanium heel spur (Figure 8(a)) is rigidly attached to the ankle joint axle. The heel spurs were made of Ti 6Al-4V ELI titanium through a direct metal laser sintering (DMLS) process, giving it a high specific strength and allowing for a hollow cross-section that is mass efficient in bending and torsion. The fatigue life of DMLS titanium is fairly low, so this part may need to be replaced more frequently than others. Each joint assembly (Figure 8(b)) contains two ball bearings that support the joint axle. Each joint assembly is attached to the lower strut of the shank assembly (Figure 7). An SLS nylon component (Figure 8(c)) covers the medial joint assembly to ensure any contact between the user's legs is glancing. An absolute magnetic encoder is housed in an SLS nylon casing (Figure 8(g)) that is attached to the joint assembly. The magnet for the encoder is glued into a pocket in the axle and rotates with it. The toe strut assembly (Figure 8(d)) is attached to the heel spur on each side by three bolts and a threaded steel insert. The heel strut assembly (Figure 8(e)) attaches to the heel strut bearing mounts (Figure 8(f)) that rotate on the joint axles. Each heel strut is attached to the heel strut bearing mount by two bolts and a threaded steel insert. The heel and toe rods run through the boots and are connected

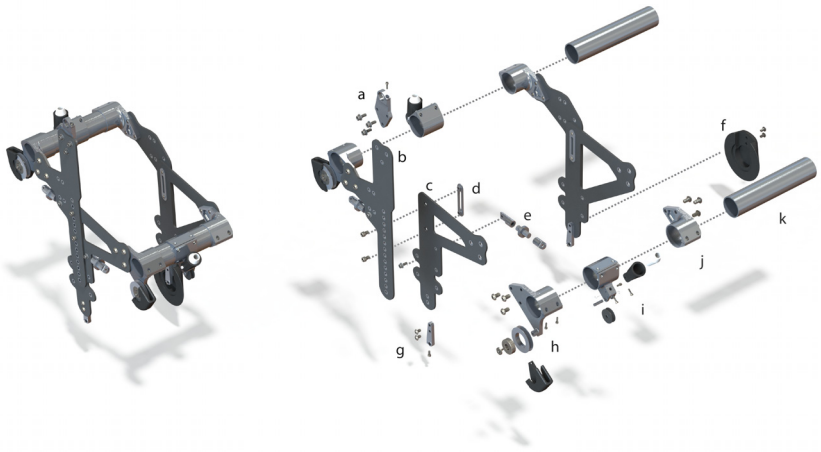

Fig. 6. Thigh segment of the exoskeleton. Assembled (left) and exploded (right) views of the thigh segment of the exoskeleton. (a) Hip joint assembly. (b) Upper thigh strut. (c) Lower thigh strut. (d) Threaded inserts. (e) Hip load cell assembly. (f) SLS nylon joint cover. (g) Knee joint assembly. (h) Lateral clamp and hip pulley assembly. (i) Knee pulley and clamp assembly. (j) Medial clamp assembly. (K) Thigh crossbars.

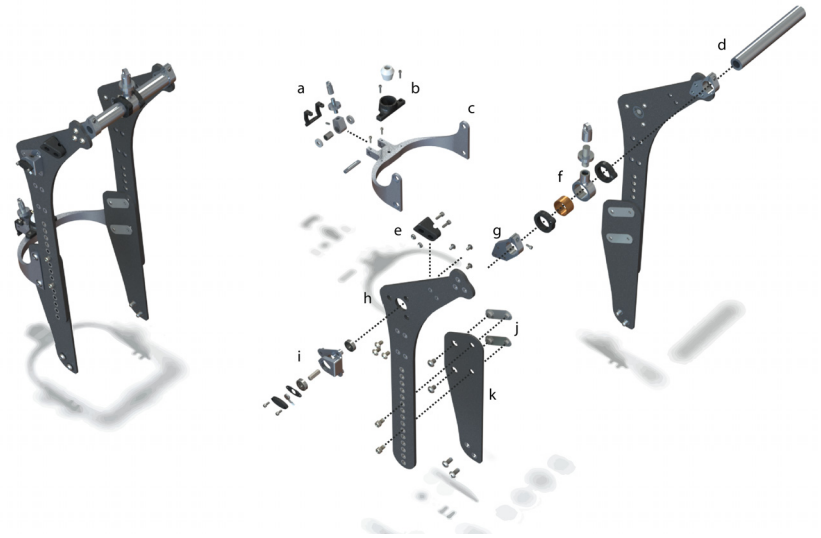

Fig. 7. Shank segment of the exoskeleton. Assembled (left) and exploded (right) views of the shank segment of the exoskeleton. (a) Knee flexion load cell assembly. (b) Ankle Bowden cable attachment. (c) Calf cuff. (d) Knee extension crossbar. (e) SLS nylon hard stop. (f) Knee extension load cell assembly. (g) Knee extension clamp. (h) Upper shank strut. (i) Knee joint assembly. (j) Threaded inserts. (k) Lower shank strut.

to the struts by steel bushings to allow for bending of the sole of the boot.

Boots in US men's sizes 5, 7, 8.5, 10, or 11 have been fit to the exoskeleton (Figure 9). Each boot has a unique toe strut assembly and heel strut assembly that are sized specifically for that boot. These components are swapped out with the boots when exchanging for different sizes. A 11.1 mm diameter, 7075 aluminum rod runs through a hole drilled in the sole of the boot to connect the two toe struts. The toe rod location is anterior to the ball of the foot directly below the toes. For previous devices, this was most comfortable and allowed the best application of plantarflexion assistance. A 12.7 mm diameter, 7075 aluminum rod runs through a hole drilled in the sole under the heel to connect the two heel struts. The heel rods were placed as posterior as possible to reduce the magnitude of the forces experienced in the toe and heel struts during torque application. The boots can be moved along the length of the toe and heel rods, which can be used to reduce medial envelope and to change the angle of the boot relative to the exoskeleton.

2.2. Exoskeleton actuation

The system is designed to apply normal forces to the user to generate torques about their joints. The inner cables and

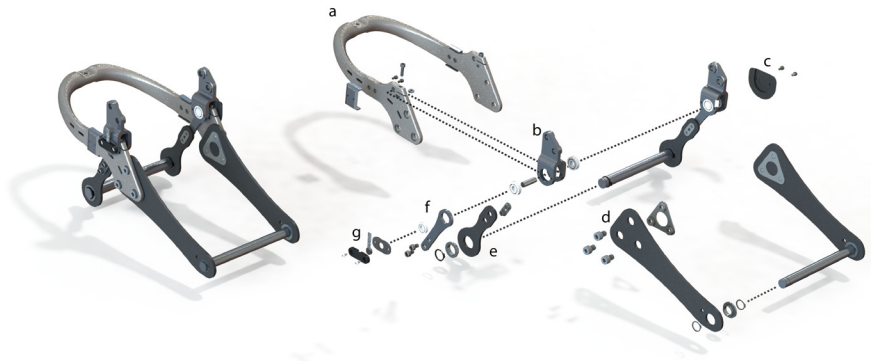

Fig. 8. Foot segment of the exoskeleton. Assembled (left) and exploded (right) views of the right foot segment of the exoskeleton. (a) Titanium heel spur. (b) Ankle joint assembly. (c) SLS nylon joint cover. (d) Toe strut assembly. (e) Heel strut assembly. (f) Heel strut bearing mount. (g) Encoder assembly.

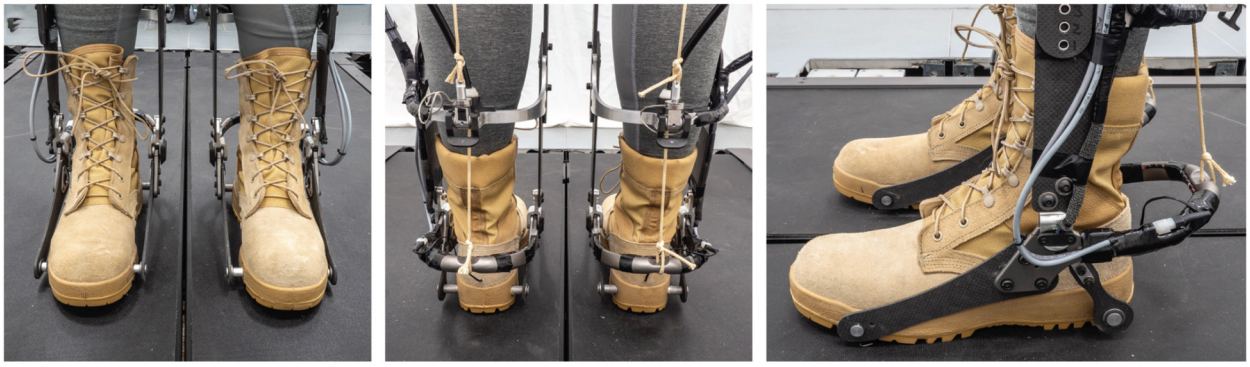

Fig. 9. Boots, toe rods, and heel rods. (a) Front view of the boots. (b) Back view of the boots. (c) Side view of the boots. Different sizes can be swapped out to fit a range of users.

outer coiled-steel conduits of the Bowden cable transmissions terminate on adjacent segments of the exoskeleton and generate equal and opposite forces on the two segments. This produces a torque about the joint but no net external force on the user (Figure 10(a)–(e)). At the knees and hips, the inner cables are routed over pulleys to allow for convenient placement of load cells to measure cable forces. Torques are then calculated by multiplying these forces by their lever arms, which are estimated using encoder measurements of joint angles and the exoskeleton's geometry. At the ankles, the inner cables terminate on the heel spurs, which are instrumented with strain gauges to sense applied torques. A more detailed description of the sensors can be found in Section 2.5.

The exoskeleton transmits torques to the user through the boots and through padded nylon straps located at the upper torso, waist, upper and lower thigh, and upper shank (Figure 11). On each segment, the straps are located far apart from each other, which increases the lever arm of each force couple and reduces the forces on the user. During knee actuation, forces applied to the boot pass through the ankle joint, producing no torque on the foot segment. During hip actuation, applied torques are designed to assist hip flexors and extensors as well as core muscles, such as erector spinae, that are typically active during biological hip flexion and extension (Winter, 1991). The chest strap and back pad apply forces to the user's torso to assist core muscles, whereas the waist strap and thigh straps apply forces to the user's pelvis and thigh to assist hip flexors and extensors.

2.2.1. Strap forces. The device is designed to apply forces normal to the user through the straps. Normal forces have been found to be more comfortable than forces applied in shear. The forces can be applied normal to the user because of the rigid frame, explicit joints, and compliant straps. When actuated, the cable force creates an equal and opposite reaction force at the pin joint, and the resulting moment is counteracted by a moment applied by the straps. The compliance of the straps allows them to shift so that they apply normal forces instead of shear forces. Because the straps are tied to the structure with paracord which can only act in tension, we can observe the line of action of the force. Based on the attachment location and the geometry of the straps relative to the legs, we can determine the force is acting primarily normal to the leg.

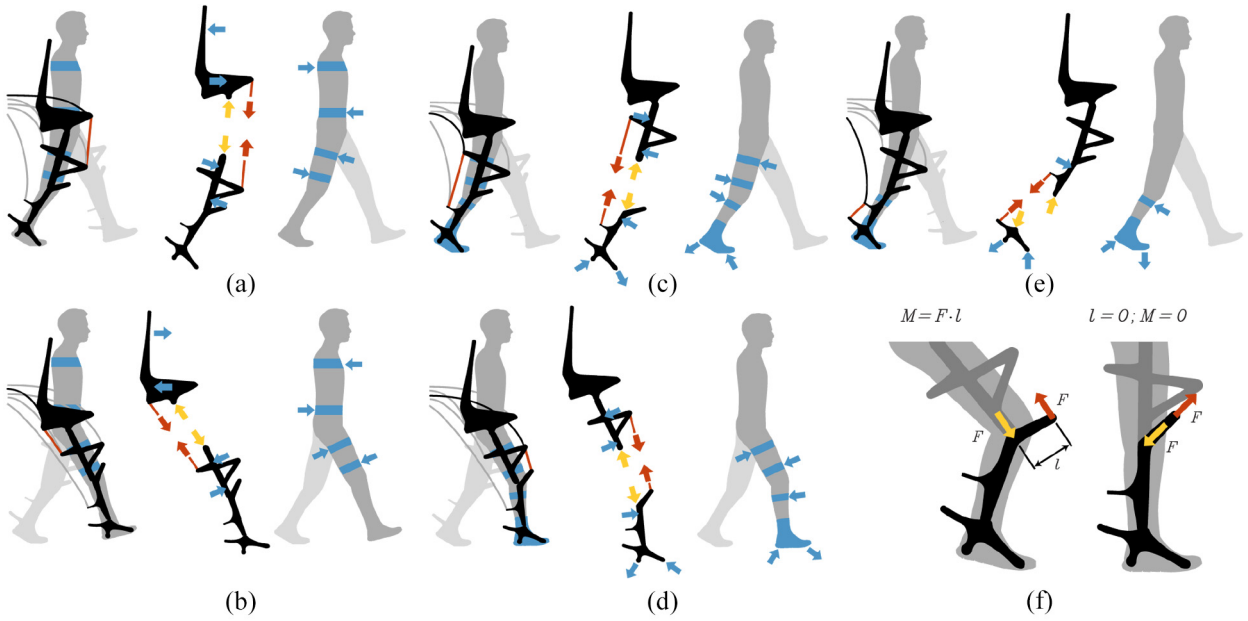

Fig. 10. Free body diagrams of exoskeleton and user. (a) Hip flexion. (b) Hip extension. (c) Knee flexion. (d) Knee extension. (e) Ankle plantarflexion. For each direction of actuation, boot and strap forces (blue arrows), cable forces (red arrows), and joint reaction forces (yellow arrows) are depicted. Each direction of actuation generates a moment about the joint by applying normal forces on the user's body. (f) Knee extension lever arm. The knee extension cable force and joint reaction force generate a moment about the knee joint when the knee is flexed. When the knee is straight, the lever arm for these forces is zero, resulting in no moment about the knee joint.

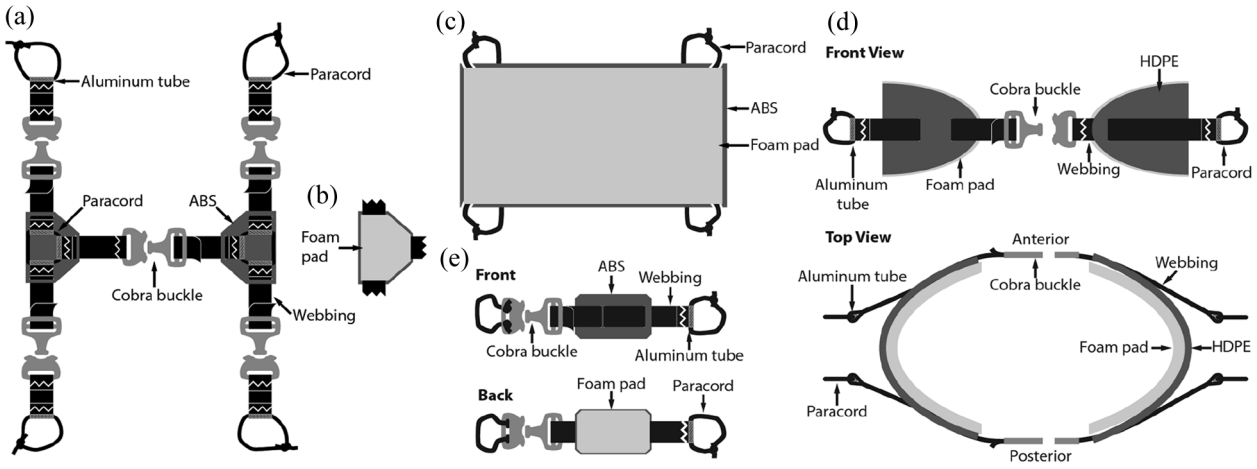

Fig. 11. Strap design. (a) Chest harness. (b) Chest harness pads. (c) Back pad. (d) Waist strap. (e) Leg strap. The straps are made of strips of webbing that run over foam pads backed with plastic to distribute the force of the straps. Each strap can be adjusted with buckles to allow for a tight fit, comfortable placement of the pads, and alignment of the exoskeleton's joints to the user's joints.

2.2.2. Loading of crossbars. The crossbars are designed to withstand combined torsional and bending loads while remaining lightweight. Their circular cross-sections are mass-optimal for the torsion they experience during actuation and allow for width adjustability (Figure 12). The back crossbar experiences large torsional loads owing to the reaction forces on the top of the back strut (Figure 12(a)). The part of the back crossbar closest to the actuated side experiences substantial torsion (indicated by its uniform green color in finite element analysis (FEA); Figure 12(a), right) and some bending, while the opposite side sees only bending. The crossbars at the thigh segment experience significant torsion owing to the loading of both the lateral and medial thigh segments during hip actuation (Figure 12(b)). The forces on the medial thigh segment are balanced by a combination of internal moments and forces in the

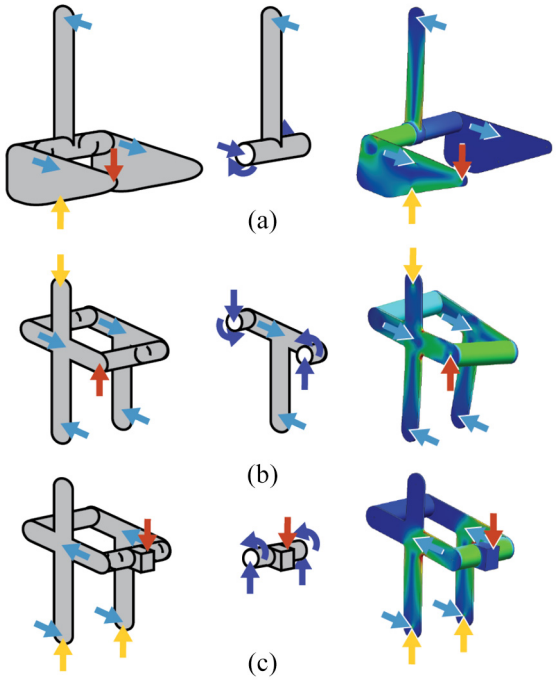

Fig. 12. Loading of crossbars on torso and thigh segments. (a) Torso segment loading during hip actuation. (b) Thigh segment loading during hip actuation. (c) Thigh segment loading during knee actuation. Strap forces (light blue arrows), cable forces (red arrows), joint reaction forces (yellow arrows), and internal forces and moments in the crossbars (dark blue arrows) are depicted. Out-of-plane forces and internal moments that do not act about the central axes of the crossbars were not included in this figure for simplicity. The rightmost images are finite element analysis (FEA) results for simplified models of the respective segments.

crossbars. The crossbars are also loaded in torsion owing to knee actuation forces, which are slightly offset from the central axis of the crossbar (Figure 12(c)). In order to withstand the torsional loads applied to each crossbar and enable width adjustability, sets of lightweight split-hub clamps connect the crossbars to the carbon fiber strut components.

2.3. Mass and geometry

The exoskeleton was designed to minimally impede the user during walking and running. The exoskeleton has a mass of 11.2 kg. When the user wears the exoskeleton, they also support some of the weight of the Bowden cables, resulting in an effective worn mass of 13.5 kg (Table 1).

The exoskeleton has a range of motion that accommodates those seen in walking and running. In the sagittal plane, it allows for 81° flexion to 23° extension at the hips, 5° extension to 115° flexion at the knees, and 59° plantarflexion to 53° dorsiflexion at the ankles. In the frontal and transverse planes, range of motion is accomplished through compliance of the structure.

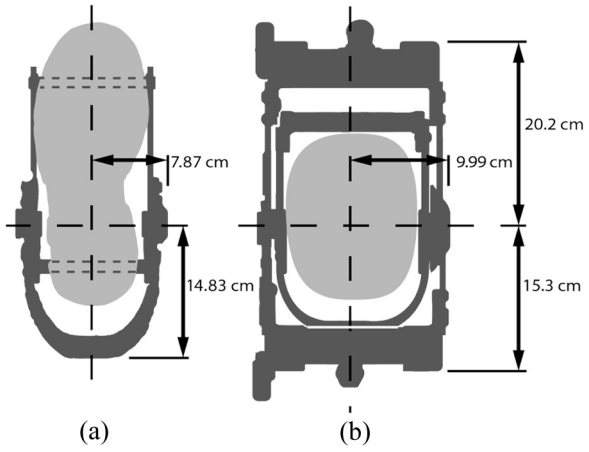

Fig. 13. Medial envelope of ankle and knee components. (a) Envelope of the left foot section. (b) Envelope of the shank and thigh sections of the left leg at the nominal width setting. Envelopes were measured from the center plane of the exoskeleton to the most medial, anterior, and posterior points of the device. The width adjustment of the crossbars at the thigh and knee can affect the medial envelope by deflecting the struts to be narrower or wider than the nominal setting.

Structures between the user's legs are low profile, with an estimated medial envelope of 7.87 cm from the center plane of the exoskeleton frame at the ankle and 9.99 cm from the center plane at the knee at the nominal width setting (Figure 13). Smooth plastic covers were placed over the medial joints of the knees and ankles to prevent catching of components and to dampen sounds during leg-to-leg contact. Although some users experienced minor leg-to-leg contact during walking and running, they were infrequent and users were able to recover quickly.

2.4. Adjustability

The exoskeleton is adjustable in height and width to fit a wide range of users (Figure 14). The lengths of the shank segment and thigh segment can be adjusted through a series of bolt holes that fasten overlapping struts. Different torso lengths can be accommodated by swapping out different back struts. The width of the exoskeleton can be adjusted continuously through tube clamp assemblies at the upper shank segment, front and back of the thigh segment, and at the back of the torso. The compliance of the struts allows them to deflect, enabling this width adjustability. Boots of different sizes can be fitted to the exoskeleton.

2.5. Sensors

The exoskeleton is instrumented to measure cable forces, joint angles, and joint torques (Figure 15). The exoskeleton uses six absolute magnetic encoders (Renishaw, RM08) to measure joint angles at the hips, knees, and ankles. For hip flexion and extension and knee extension, the forces in the

Table 1. Mass estimates for segments of the exoskeleton. Measurements for the feet, shanks, and thighs include the mass of both legs. Structure masses were estimated from the CAD model of the exoskeleton. The masses of the straps and boots (size 10) were measured directly. Bowden cable masses were determined by measuring the exoskeleton with and without the cables attached. The "wiring/other" mass includes the sensors, wiring, breakout boards, and errors in the estimation of the structure mass from the CAD model. The D-Sub cables at the hips were measured directly, while the remaining mass was distributed with 1/24 of the mass per shank and per foot, 1/6 of the mass per thigh, and 1/2 of the mass at the torso to approximately reflect the distribution of electronic components on the exoskeleton.

	Structure mass (kg)	Straps and boots (kg)	Bowden cables (kg)	Wiring/ other (kg)	Segment mass (kg)
Feet	1.2	1.4	0.0	0.1	**2.7**
Shanks	1.7	0.2	0.4	0.1	**2.4**
Thighs	2.4	0.4	0.7	0.4	**3.9**
Torso	2.2	0.6	0.7	1.0	**4.5**
Total	**7.5**	**2.6**	**1.8**	**1.6**	**13.5**

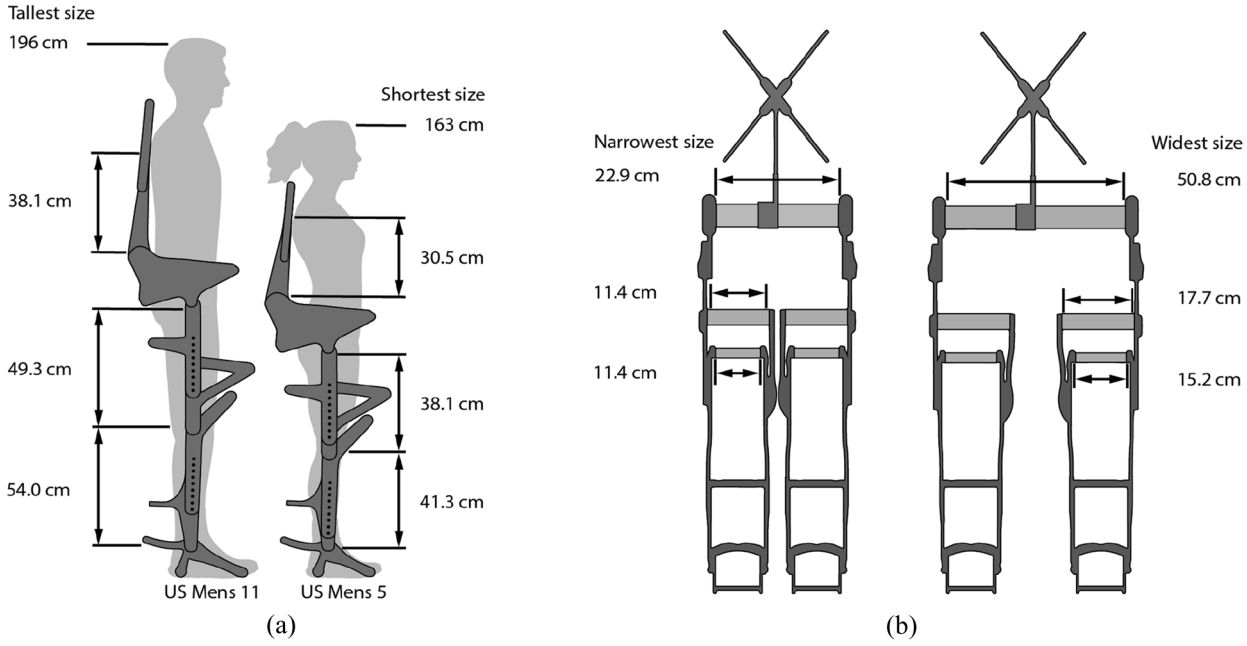

Fig. 14. Size adjustability of the exoskeleton. (a) Length adjustability of the exoskeleton. The back strut on the torso segment can be swapped for different lengths in 1.9 cm increments, whereas the thigh and shank segments can be adjusted in 1.3 cm increments. Boots can be fitted in US men's sizes 5, 7, 8.5, 10, or 11. (b) Width adjustability of the exoskeleton. The width of the exoskeleton is continuously adjustable. This adjustability relies on deflection of the upper shank and thigh struts.

inner Bowden cables are measured with load cells (Futek, FSH03904). Lighter duty load cells (Omega, LC201-300) measure cable forces for knee flexion. The load cell and encoder outputs are used to calculate joint torques for the hips and knees. Strain gauges (Omega, MMF003129) in a full Wheatstone bridge are located on the heel spur to measure the torque applied about the ankle. The strain gauge and load cell signals are amplified off-board (Futek, FSH03863).

All sensor signals are transmitted as analog voltages from the exoskeleton to the off-board control hardware. The sensor leads at the knees and ankles are crimped to flexible cables (Igus, chainflex) that are routed up the leg to the waist struts. The flexible cables are routed to minimize both cable strain and dangling loops, while allowing full range of motion and length adjustment of the shank and thigh segments. At the waist struts, the sensor cables are secured using aluminum clamps with rubber padding strips to provide strain relief for the connections at the breakout boards. To ground the shielding, brass clamps contact the cable shielding and connect to the ground of the breakout boards. The sensor cables are connected to screw-terminal breakout boards (BiPOM, BRKSD44HDMV2-C) mounted posterior to the hip joints with SLS nylon mounts. These terminals connect to 20-foot long HD-44 D-Sub cables (Digi-Key) that run from the waist struts to an off-board breakout board (BiPOM, BRKDD44HDF-R-FT) which is connected to the real-time target machine through BNC cables (Digi-Key).

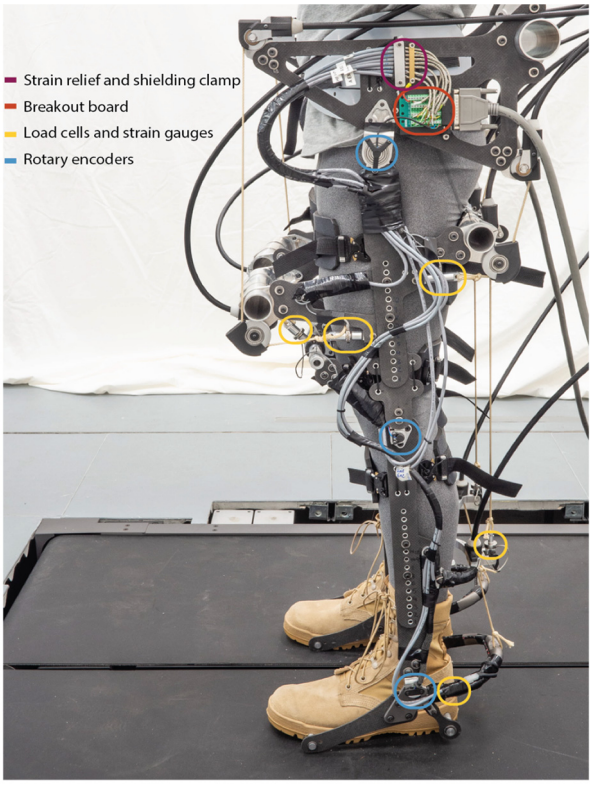

Fig. 15. Sensors and wiring of the exoskeleton. The exoskeleton end effector is equipped with encoders to measure joint angles at each joint, load cells for measuring cable force for the hips and knees, and strain gauges for measuring torques at the ankle. Sensor cables are secured by strain relief and connect to D-Sub cables through a breakout board at the hips. These D-Sub cables transmit sensor data to the offboard control hardware.

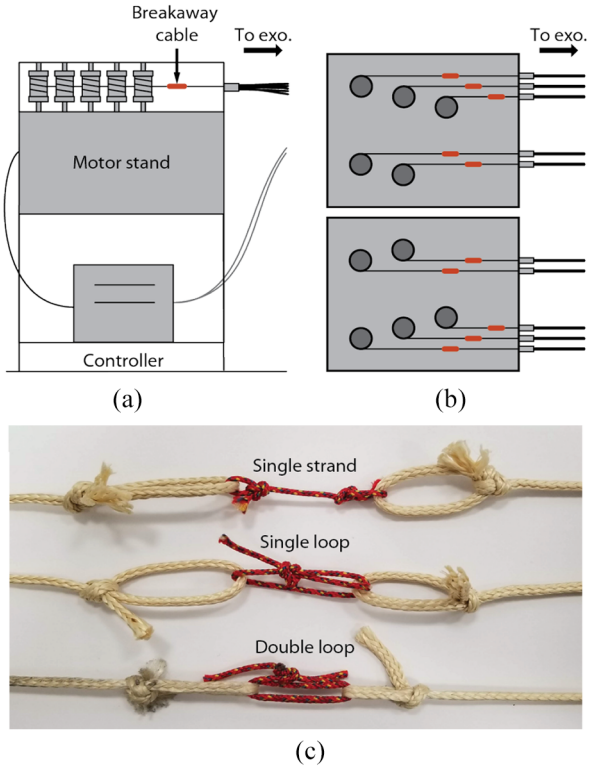

Fig. 16. Breakaway cable for limiting applied cable force. (a) Side view of the motor stand. (b) Top view of the motor stand. (c) Close-up of three different ways to tie the breakaway corresponding to different strength requirements. The breakaway cable is a thinner cable that breaks if the applied cable force is too high. For each direction of actuation, the breakaway cable is located in series between the motor and the Bowden cable routed to the exoskeleton.

2.6. Safety

To protect the user, the exoskeleton design includes a variety of safety features. The knee extension lever arm geometry ensures that no torque can be produced by actuation forces when the knee is straight, which protects against hyperextension injuries (Figure 10(f)). Mechanical hard stops prevent hip flexion, hip extension, and knee extension from exceeding the allowed range of motion. Each inner Bowden cable is tied in series with a thinner breakaway cable (Figure 16). This thinner cable breaks if too large of a force is applied, which disconnects the motor from the exoskeleton. Safety measures in the control software ensure no torques are applied if the device joint angles are beyond the prescribed range of motion for the intended gait. A maximum torque limit is enforced by the software. The motors can be shut off with emergency-stop buttons located near the user and the operator.

2.7. Off-board hardware

The exoskeleton uses off-board motors and control hardware. The motor unit (Human Motion Technologies) utilizes ten 7.0 kW motors (Kollmorgen, AKM74P) driven by 10 motor drivers (Kollmorgen, AKD-P02407). The motor unit is positioned behind an instrumented treadmill (Bertec). The motors are connected to a real-time target machine (Speedgoat) running a Simulink Real-Time controller (MATLAB) at 2,500 Hz and filtering sensor data at 100 Hz. Each motor is connected to the exoskeleton end effector by a flexible Bowden cable made up of an inner cable (West Marine, V-12 Vectran Single Braid) running through an outer coiled-steel conduit (Lexco, 415310-00). More detailed part descriptions and part costs are included in the bill of materials (Extension 4).

2.8. Materials and fabrication

The exoskeleton is composed of both commercially available and custom components. The strut components were waterjet cut (Waterjet Cutting Inc.) from carbon fiber sheets (DragonPlate, 1/8” and 3/16” quasi-isotropic sheets). Custom aluminum and steel components were machined in-house at Carnegie Mellon University, at Stanford University or commercially by ProtoLabs. The

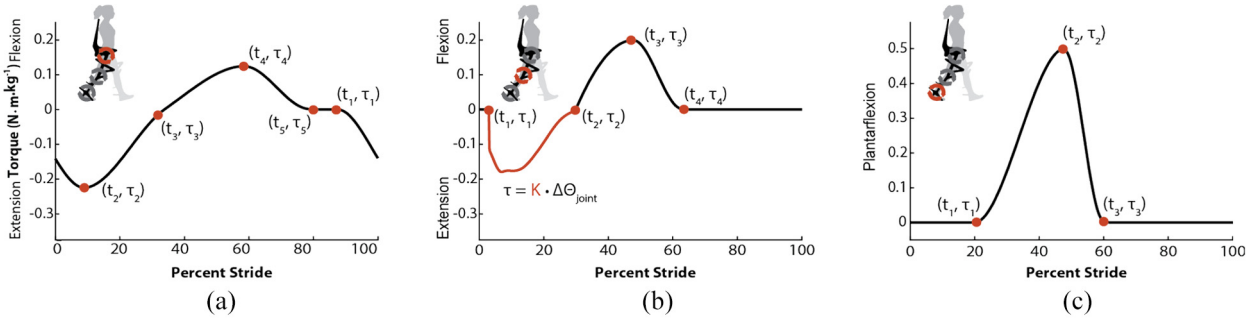

Fig. 17. Desired torque profiles with defined nodes. (a) Desired torque profile for hip actuation. (b) Desired torque profile for knee actuation. (c) Desired torque profile for ankle actuation. Each profile is plotted as a function of percent stride. For knee extension during stance (B, in red), desired torque is commanded as a virtual spring, with torque proportional to the measured knee angle relative to the knee fully extended. The timing onset and offset of this spring are determined by nodes. For torque tracking tests, the nodes were selected by an operator to ensure user comfort and were not evaluated for metabolic benefit or any other functional outcome. These profiles were applied in the evaluation of comfort, torque tracking, and torque application during different walking conditions.

titanium heel spurs were additively manufactured through DMLS (ProtoLabs). The strap assemblies were developed in-house at Carnegie Mellon University (Figure 11). Each boot (McRae Footwear, Style #8189) has two aluminum rods inserted transversely through the sole beneath the heel and toes (Figure 9). A CAD model of the exoskeleton is given in Extension 3 and a bill of materials is given as Extension 4.

2.8.1. Strap fabrication. The straps were designed to comfortably transmit forces to bony landmarks. The chest harness is made of 25.4 mm wide webbing that runs over two pads on the user's chest (Figure 11(a)). Straps lie above and below the user's shoulders and are tied to the shoulder struts with paracord, and one strap runs horizontally across the user's chest. Each strap is adjustable with Cobra buckles (AustriAlpin) to allow for a tight fit and comfortable placement of the pads. We have found that the pads are most comfortable when placed high on the chest such that they do not restrict natural chest expansion during breathing. The chest harness pads are made of foam backed with 1.6 mm thick ABS to distribute the force of the straps (Figure 11(b)). The back pad is made of 38.1 mm thick foam backed with 0.8 mm thick ABS (Figure 11(c)). The back pad is tied to the shoulder struts with paracord. The pad was designed to be wide enough to ensure contact on the user's scapulae. The waist and leg straps are made of 25.4 mm wide webbing and are tied to the struts with paracord. At the waist, the straps run over foam pads backed with 1.6 mm thick HDPE that rest on the user's iliac crests (Figure 11(d)). On the legs, the straps run over foam pads backed by 0.8 mm thick ABS (Figure 11(e)). The webbing is reinforced with 6.4 mm diameter aluminum tubes at the interface to the paracord. Cobra buckles provide adjustability at the front and back of the torso, waist, and legs, which allows the exoskeleton's joints to be aligned with the user's joints.

3. Control

The exoskeleton's controller is determined by joint torque profiles defined at the hips, knees, and ankles. If torque is desired for a certain direction of actuation, the corresponding motor applies the torque. If the desired torque is zero or the antagonist motor is active, the motor tracks the user's joint angles without applying torques. Desired torque profiles can be defined by an operator or algorithm (Figure 17). During walking, we defined these profiles as functions of percent stride. For the ankles and knees, this was calculated as the time since the last heel strike divided by the average stride time. Average stride time was calculated by measuring the time between heel strikes and averaging over the last five strides. For the hips, we apply torques during heel strike, which results in discontinuities of desired torque if stride time is reset at heel strike. Therefore, the hip profile begins at 84% of stride after heel strike, which corresponds to a period where no torque is applied, and may therefore be slightly out of phase with other joint torques. With the exception of knee extension, profiles are generated as piecewise cubic hermite interpolating polynomial (*pchip*) splines defined by nodes that can be changed by an operator or algorithm. For knee extension during stance, torque is commanded as a virtual spring, with torque proportional to knee angle, which is considered to be zero when the knee is straight. The onset of this state-based controller is commanded as a function of percentage stride, whereas the offset is commanded as either a function of percentage stride or when the knee joint angle reaches zero degrees. As the knee joint angle is not necessarily zero at the start of the state-based controller, desired torque will instantaneously change at the onset.

When applying torques, the motors are controlled using proportional control with feedforward velocity and iterative learning compensation, similar to the methods described in Zhang et al. (2015). Iterative learning is feed-forward error compensation to remove systematic error. The error is

calculated for each time index and then added to the control signal during the next stride. The control signal is

$$u(i,n) = K_{\mathrm{p}} \cdot e(i,n) + K_{\mathrm{v}} \cdot \dot{\theta}_{\mathrm{m}}(i,n) + u_{\mathrm{L}}(i+D,n) \quad (1)$$

$$u_{\mathrm{L}}(i,n+1) = \beta \cdot u_{\mathrm{L}}(i,n) + K_{\mathrm{L}} \cdot e(i,n) \quad (2)$$

For the hips and knees, e is the measured cable force error, where $e = F_{\mathrm{des}} - F_{\mathrm{meas}}$ is the difference between the desired cable force and the measured cable force. The desired cable force is calculated from the desired torque and the estimated lever arm. For the ankles, e is the torque error where $e = \tau_{\mathrm{des}} - \tau_{\mathrm{meas}}$. Torque is used for the ankles because applied torque is measured directly.

Here K_{p} is the proportional gain, K_{v} is the gain on the motor velocity, and $\dot{\theta}_{\mathrm{m}}$ is the motor velocity corresponding to the measured joint velocity. Here u_{L} is a feed-forward error compensation term for each time index of the torque profile, β is a decay term where $\beta = 0.99$, K_{L} is a gain on the torque error, D is an estimate of the time delay between the command and the application of torque, i is the time index, n is the current stride, and $n+1$ is the next stride. We initially found systematic error at the onset of torque even with iterative learning, so the controller also preemptively reduces slack in zero-torque mode immediately before the onset of torque.

When not applying torque, the motors track desired positions based on exoskeleton joint angles using a closed-loop proportional controller. Desired motor position is determined from an experimental mapping of the joint angle to the motor angle. To ensure the device does not impede the user's natural motions, the desired cable length has an additional 2.54 cm of slack.

While tracking both motor positions and torques, control signals are sent to the motor driver, which operates in velocity control mode.

4. Benchtop experiments

We conducted a series of experiments to evaluate the capabilities of the exoskeleton. For each direction of actuation, we tested its bandwidth and maximum torque and estimated its maximum power and maximum joint velocity. To evaluate user impedance, we quantified the compliance of the exoskeleton in hip adduction and abduction, hip internal and external rotation, spinal lateral bending, and spinal axial rotation.

4.1. Benchtop testing setup

Maximum torque and bandwidth tests were conducted with the exoskeleton strapped to a rigid aluminum test stand to avoid injuring a user during high-torque or high-cycle loading (Figure 18). The frame was about the size and proportions of an adult user, with the ankle at 0°, knee at 45°, and hip at 0°. The knee was flexed at 45° to maximize the knee extension lever arm for high torque application. For benchtop testing, torques were commanded as a function of time.

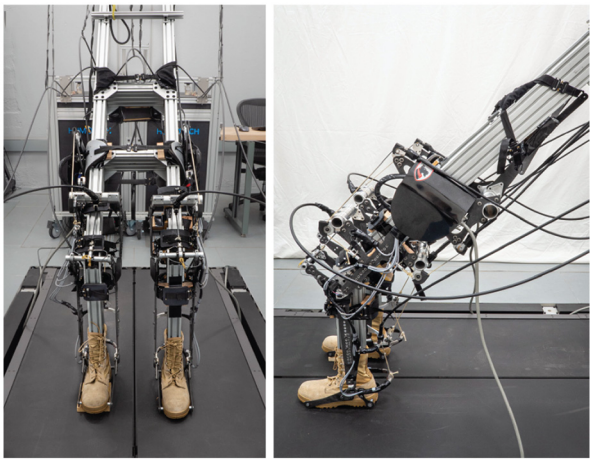

(a) (b)

Fig. 18. Rigid benchtop test stand. (a) Front view. (b) Side view. An aluminum t-slotted frame (80/20) was layered with wood at strap locations to ensure a secure fit of the device during testing. The knee joint of the exoskeleton was flexed at 45° to ensure the lever arm was large enough for maximum torque tests.

4.2. Bandwidth tests

Closed-loop torque bandwidth was measured for each direction of actuation (Figure 19 (a) and (b), and Multimedia extension 5). During these tests, the exoskeleton was controlled using closed-loop proportional control without any iterative learning. A sinusoidal torque profile that oscillated between 10% and 60% of maximum torque was commanded. Optimal walking assistance has been found at roughly 60% of biological torque (Zhang et al., 2017); therefore, we could reasonably expect an optimal profile for running to reach these magnitudes.

The profile was initially applied with a frequency of 1 Hz, which was then discretely increased by 1 Hz until the bandwidth was reached. The bandwidth for each direction of actuation was defined as the frequency at which the gain reached −3 dB or when the phase offset reached 150°. A movie including bandwidth testing is included as Multimedia extension 5. Bandwidth values tested on a human user are lower than when a device is tested on a rigid test stand (Witte et al., 2017), so we expect bandwidth may be slightly lower in practice.

4.3. Maximum torque tests

The maximum torque capabilities of the exoskeleton were tested. For each direction of actuation, the maximum torque was commanded 10 times as a step and held for 0.25 seconds each (Figure 19(c), Multimedia extension 5), which is similar to the duration of stance time during running (Novacheck, 1998).

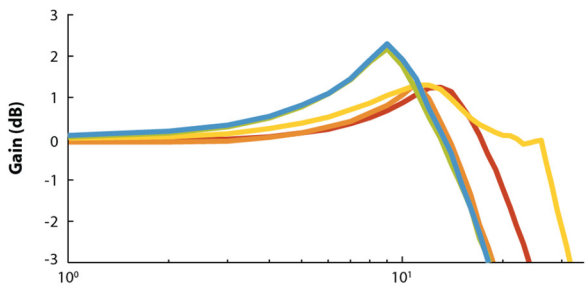

(a)

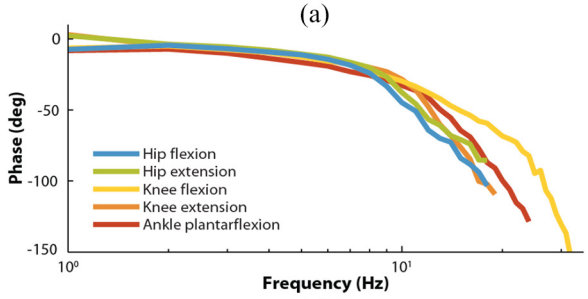

(c)

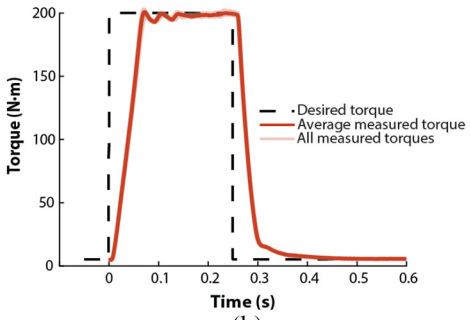

(b)

	Torque (N·m)	Bandwidth (Hz)	Velocity (rad·s⁻¹)	Power (kW)
Hip flexion	200	18	23	4.6
Hip extension	200	18	25	4.9
Knee flexion	140	31	17	2.8
Knee extension	250	18	31	7.4
Plantarflexion	200	23	36	7.0

(d)

Fig. 19. Results from benchtop testing. (a) Amplitude response Bode plot from bandwidth tests. (b) Phase response Bode plot from bandwidth tests. Each direction of actuation was tested separately with the exoskeleton strapped to a rigid test stand (Figure 18). (c) Example of maximum torque testing for ankle plantarflexion. For each direction of actuation, torque was measured during maximum torque tests on a rigid test stand. Desired torque (black, dashed) was commanded as a step 10 times for 0.25 seconds each. All measured torques for the 10 trials are shown (light red) as well as the mean of the trials (dark red). (d) Torque, bandwidth, velocity, and power capabilities. Results of benchtop tests (maximum torque and bandwidth) and estimates based on motor specifications (maximum speed and power) for each direction of actuation.

4.4. Maximum joint power estimations

The maximum exoskeleton joint power was calculated from data obtained in the maximum joint torque tests and motor specifications. This metric would have been too difficult to safely and reliably test based on joint measurements alone. The maximum joint power, $P_{\mathrm{j,max}}$, was calculated as the measured, maximum joint torque, $\tau_{\mathrm{j,max}}$, multiplied by the largest joint velocity the motors can maintain while applying the maximum joint torque, ω_{j}:

$$P_{\mathrm{j,max}} = \tau_{\mathrm{j,max}} \cdot \omega_{\mathrm{j}} \tag{3}$$

We determined the largest available motor velocity at the maximum joint torque, ω_{m}, through the motors' torque–velocity curves operating at 660 V and at the de-rotated, actual current measured during the maximum joint torque experiments. To find the corresponding joint velocity, ω_{j}, the motor velocity, ω_{m}, was multiplied by the ratio of the motor drum radius, r_{m}, to the joint lever arm, r_{j}:

$$\omega_{\mathrm{j}} = \omega_{\mathrm{m}} \cdot \frac{r_{\mathrm{m}}}{r_{\mathrm{j}}} \tag{4}$$

4.5. Maximum joint velocity estimations

The maximum joint velocity, $\omega_{\mathrm{j,max}}$, was calculated using the motor's no-load velocity, $\omega_{\mathrm{m,nl}}$. The no-load velocity is a reasonable estimate of the system's maximum velocity, since friction in the transmission would produce only a small load on the motor when exoskeleton joint torque was zero:

$$\omega_{\mathrm{j,max}} = \omega_{\mathrm{m,nl}} \cdot \frac{r_{\mathrm{m}}}{r_{\mathrm{j}}} \tag{5}$$

The maximum joint velocity, $\omega_{\mathrm{j,max}}$, was calculated from the no-load speed, whereas the joint velocity from the power calculation, ω_{j}, was calculated from the current drawn during the maximum joint torque experiments. The maximum joint velocity is larger than the largest available velocity while at the maximum joint torque.

4.6. Torque, bandwidth, velocity, and power capabilities

In benchtop tests, the system applied torques similar to those seen in uphill running (male, 80kg, 12° incline, 3.0 m/s; Roberts and Belliveau, 2005) and demonstrated high bandwidth capabilities for accurate application of torques during walking (Figure 19). The exoskeleton has estimated power and velocity capabilities that exceed those seen in uphill running (Roberts and Belliveau, 2005).

4.7. Exoskeleton compliance tests

4.7.1. Methods. We tested the exoskeleton's compliance in hip abduction, hip rotation, spinal lateral bending, and spinal axial rotation (Figure 20). Forces were applied at

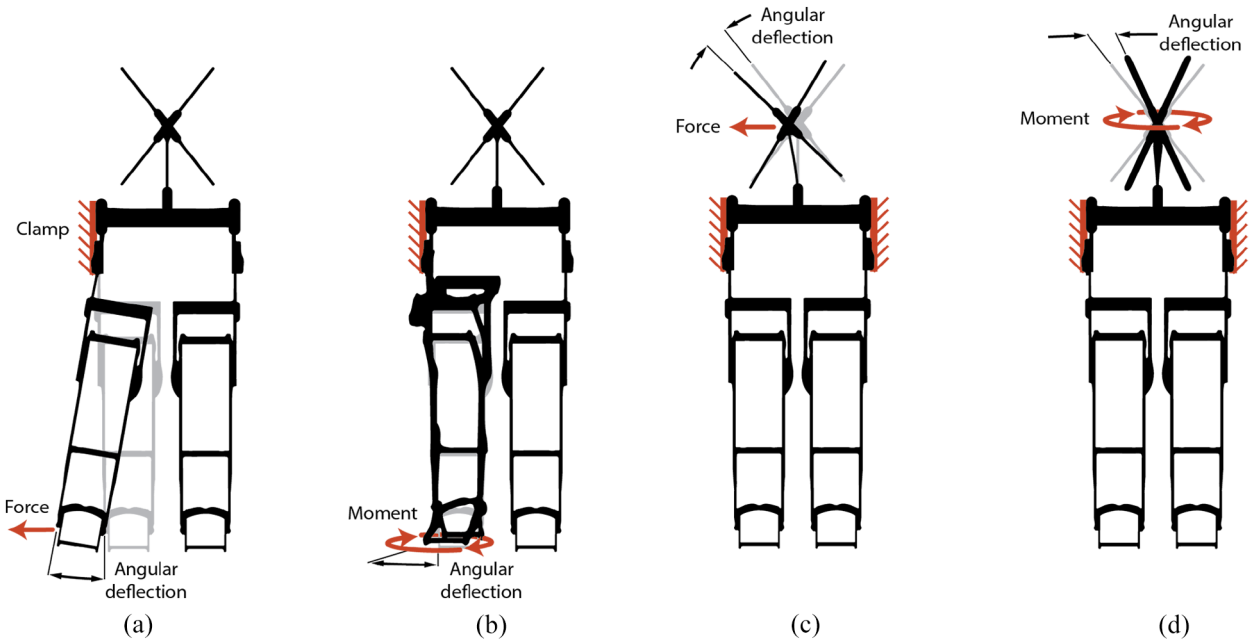

Fig. 20. Compliance testing setups. (a) Hip adduction and abduction testing setup. (b) Hip internal and external rotation testing setup. (c) Spinal lateral bending testing setup. (d) Spinal axial rotation testing setup. The compliance was determined by clamping part of the structure, applying a force or a moment, then measuring the angular deflection.

different locations on the exoskeleton and the resulting deflection angle was measured with a digital angle gauge. The hip abduction and hip rotation tests were performed with the exoskeleton's waist strut clamped to a rigid structure, and the device was sized for a 173 cm tall participant. In the hip abduction test, a mediolateral force (11.1, 22.2, and 33.4 N) was applied to the ankle joint component (82 cm from hip joint) of one leg of the exoskeleton (Figure 20(a)). In the hip rotation test, two equal and opposite mediolateral forces (22.2, 44.4, and 66.6 N) were applied at a fixed distance (16.5 cm) from the center of the ankle joint (Figure 20(b)). Spinal lateral bending and axial rotation tests were done with the back bar clamped to a rigid structure. In the spinal lateral bending test, a mediolateral force (22.2 and 44.4 N) was applied to the top of the back strut (29.5 cm from back crossbar; Figure 20(c)). In the spinal axial rotation test, two equal and opposite anteroposterior forces (22.2 and 44.4 N) were applied at a fixed distance (12.7 cm) from the center of the back strut (Figure 20(d)). For each test, the applied forces were multiplied by their corresponding lever arms to determine the applied moment. The applied moments were then divided by the measured deflection angles to determine the stiffnesses and then averaged across the tested conditions. These evaluations did not take into account the added compliance of the strap interface, and therefore represent a lower bound of device compliance.

4.7.2. Results. The exoskeleton is compliant, with low stiffness in hip adduction and abduction (1.08 Nm/degree), hip internal and external rotation (1.02 Nm/degree), spinal axial rotation (0.38 Nm/degree), and spinal lateral bending (0.87 Nm/degree). Compliance of the straps allows for some relative motion between the user and the exoskeleton, reducing the effective stiffness to below these values.

5. Human subject tests

We conducted a series of experiments to evaluate the effect of wearing the device. To evaluate user impedance, we measured the metabolic effect of wearing the device while walking. We conducted user experiments to verify the device was sufficiently adjustable and comfortable to walk in. These experiments were conducted on a total of 14 participants. Three of these participants are considered experienced users and are also authors of this article.

All user experiments were approved by the Stanford University Institutional Review Board and the US Army Medical Research and Materiel Command (USAMRMC) Office of Research Protections. All participants provided written informed consent before their participation as required by the approved protocol.

5.1. Adjustability, donning, and doffing

We conducted several user experiments to evaluate adjustability, donning, and doffing. For 10 inexperienced participants (7 female, 3 male, 163–182 cm, 48–77 kg), the amount of time to adjust, don, and doff the exoskeleton was recorded (Multimedia extension 6).

5.1.1. Adjustability results. A total of 23 people, ranging from 163 to 196 cm in height, have walked in the exoskeleton. This corresponds to the 5th to the 99th percentile of

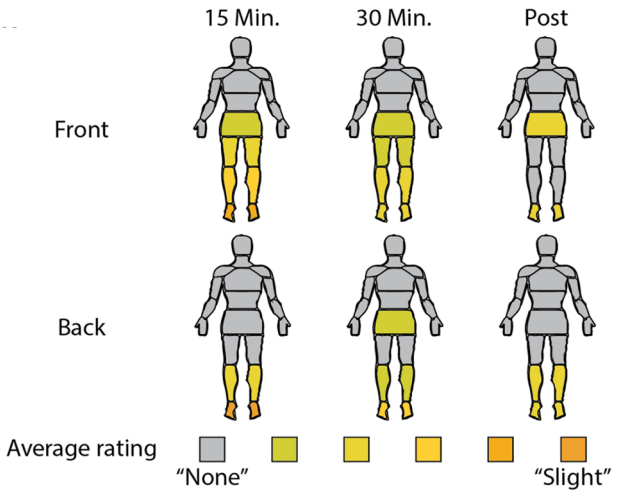

(a)

Participant	Pre	15 min.	30 min.	Post
1	7	4	3	6
2	6	5	5	7
3	7	5	6	7
4	7	6	6	7
5	7	4	5	6
Average	**6.8**	**4.8**	**5**	**6.4**

"Extremely uncomfortable" 1 → 7 "Extremely comfortable"

(b)

Fig. 21. Comfort evaluations of each segment and overall comfort. Five users rated their pain, soreness, and discomfort before wearing the device to determine baseline ratings (Pre), after walking in the device for 15 min without torque (15 min), after walking in the device for an additional 15 min with torque (30 min), and after getting out of the device (Post). (a) Average rating of pain, soreness, or discomfort for each body segment. Users ranked their pain, soreness, or discomfort as none, slight, moderate, severe, or extreme. (b) Ratings of overall comfort. Users evaluated their overall comfort on a scale of 1–7 with 1 being extremely uncomfortable and 7 being extremely comfortable.

US males, and the 57th to 99th percentile of US females (CDC, 2015).

5.1.2. Donning and doffing results. Users are able to quickly don and doff the exoskeleton. For 10 first-time users, donning and adjusting the exoskeleton required the help of another person and took an average of 31.8±10.3 min. When the exoskeleton was already adjusted to the correct size, experienced users could don without assistance in under 5 min Doffing the exoskeleton took an average of 1.07±0.18 min.

5.2. Comfort

5.2.1. Methods. Five inexperienced participants (3 female, 2 male 163–182 cm, 48–75 kg) evaluated the comfort of wearing the device. None of the participants were authors or otherwise involved with conducting this study. The participants walked for 15 min without torque and then 15 min with torques applied. The applied torques were hand-tuned profiles scaled by body mass (Figure 17). The participants evaluated the comfort of the device by rating their overall comfort as well as rating their pain, soreness, or discomfort for individual body segments (Corlett and Bishop, 1976). The evaluations were taken before donning the device (Pre), after walking for 15 min without torque (15 min.), after walking for an additional 15 min with torque (30 min.), and after doffing the device (Post). The evaluation form can be found as Extension 7. Torque application during these tests was intended to help assess the interface between the device and participant, not as an assessment of the quality of the assistance profiles.

To assess the overall impact of the device, users rated the overall comfort on a scale from 1 to 7, with 1 being "extremely uncomfortable" and 7 being "extremely comfortable."

Users then rated any pain, soreness, or discomfort at each segment as none, slight, moderate, severe, or extreme. Ratings for each segment were averaged across participants. The average baseline ratings were then subtracted from the 15 min., 30 min., and Post ratings.

5.2.2. Results. In general, users found walking in the device to be comfortable. On a scale of 1–7, users rated the device 5 out of 7 on average after 30 min of walking in the device (Figure 21). For segment evaluations, users rated most segments with ratings of "none" or "slight," and no user rated any segment worse than "moderate" (Figure 21). The back of the feet had the highest rating on average, with a median rating of "slight" discomfort.

5.3. Metabolic impact tests

5.3.1. Methods. We experimentally evaluated the metabolic impact of walking in the device for nine users (3 female, 6 male, 164-196 cm, 60-102 kg, 3 experienced). We measured the metabolic cost of quiet standing, walking in boots, and walking in the device while no torques were applied. Walking trials were conducted at 1.25 m/s on an instrumented treadmill equipped with handrails. Metabolic measurements were made using indirect calorimetry

Table 2. Metabolic impact of the exoskeleton. For nine users (three experienced: 5, 8, and 9), metabolic cost was measured using indirect calorimetry during three conditions: standing while not wearing the exoskeleton (Quiet standing), walking while wearing boots but not in the exoskeleton (Walking in boots), and walking in the exoskeleton while no torques are being applied (Walking in exo.).

Participant	Mass (kg)	Quiet standing (W/kg)	Walking in boots (W/kg)	Walking in exo. (W/kg)
1	60	1.54	4.63	6.48
2	64	1.77	4.77	6.28
3	66	1.27	4.46	5.84
4	77	1.52	4.48	5.67
5	86	1.50	4.56	5.34
6	102	1.86	4.63	5.77
7	75	1.90	5.28	6.65
8	64	1.52	4.54	5.32
9	82	1.52	4.37	5.03
Average	**75**	**1.60**	**4.64**	**5.82**

(Cosmed). Participants were instructed to fast for 4 h before the experiment. Each evaluation lasted 6 min, with a 5 min rest between evaluations. The calculated metabolic cost for each condition was the average over the last 3 min of the measurement. Measurements were normalized by body mass and are reported in W/kg. Quiet standing was subtracted when calculating the percentage change in metabolic cost.

5.3.2. Results. For nine users, walking in the device increased their metabolic cost by 1.18 ± 0.39 W/kg (mean $\pm$ standard deviation) compared with walking in boots (Table 2).

6. Torque application experiments

We conducted a series of experiments to evaluate the device's ability to apply torques to the user during normal walking as well as during different gait conditions. We evaluated torque tracking during multi-joint actuation as well as during single-joint actuation. We also applied hip–knee–ankle torques to one user during slow, fast, incline, and weighted walking as well as while running.

6.1. Torque tracking during walking

6.1.1. Methods. We tested the exoskeleton's ability to track torques during walking. Desired torque profiles were hand-tuned and scaled by body weight to ensure novice participants could walk comfortably (Figure 17). For this test of robotic system performance, we did not evaluate effects on biomechanical outcomes. Five users (3 female, 2 male, 164–188 cm, 60–86 kg) walked in the exoskeleton at 1.25 m/s while torques were applied. To find the total torque-tracking error, the root-mean-square (RMS) error for all strides in the trial was calculated. To evaluate the systematic error, the RMS error between the average measured torque profile and the desired torque profile was calculated. Torque-tracking capabilities were assessed for multi-joint torque profiles with peak torques up to 0.5 Nm/kg at the hips, knees, and ankles over three min of walking. Multi-joint torque magnitude was limited for participant comfort. To assess torque tracking for higher applied torques, one experienced user (male, 188 cm, 82.5 kg) walked with single joint actuation up to 50 Nm corresponding to 0.61 Nm/kg for 3 min.

6.1.2. Results. The exoskeleton can accurately apply torques during walking (Figure 22). For five users, torque tracking error was evaluated while walking with multi-joint actuation (Figure 22(a)–(c)). During multi-joint actuation at the hips, knees, and ankles, the total RMS error was on average 0.0272 Nm/kg (9% of peak torque for that joint) whereas the systematic RMS error was on average 0.0138 Nm/kg (4% of peak torque for that joint) over 3 min of walking (Figure 22(g)). Knee extension torque was defined by a virtual spring resulting in step-to-step variations in both desired and measured torque between 5% and 30% of stride (Figure 22(b)).

To evaluate the device's ability to track larger torques during walking, one user walked with single-joint actuation with peak torques of up to 0.61 Nm/kg (Figure 22(d)–(f)). The total RMS error for the trial was on average 0.0379 Nm/kg (6% of peak torque for that joint), whereas the systematic RMS error was on average 0.0171 Nm/kg (3% of peak torque for that joint) over 3 min of walking (Figure 22(g)). For all trials, the profiles were chosen to characterize the torque-tracking capabilities of the system; no biomechanical measurements were taken.

6.2. Torque application during different conditions

We applied hip–knee–ankle torques to one user during slow, fast, incline, and weighted walking as well as while running to show that the device has the potential to provide assistance in a variety of conditions. One experienced user (male, 188 cm, 86 kg) walked and ran with torques applied to the hips, knees, and ankles during various conditions. In all conditions, the assistance profiles were the same as the comfort evaluation and multi-joint torque tracking (Figures 17 and 22(a)–(c)). The user walked at 0.75, 1.25, and 1.75 m/s,

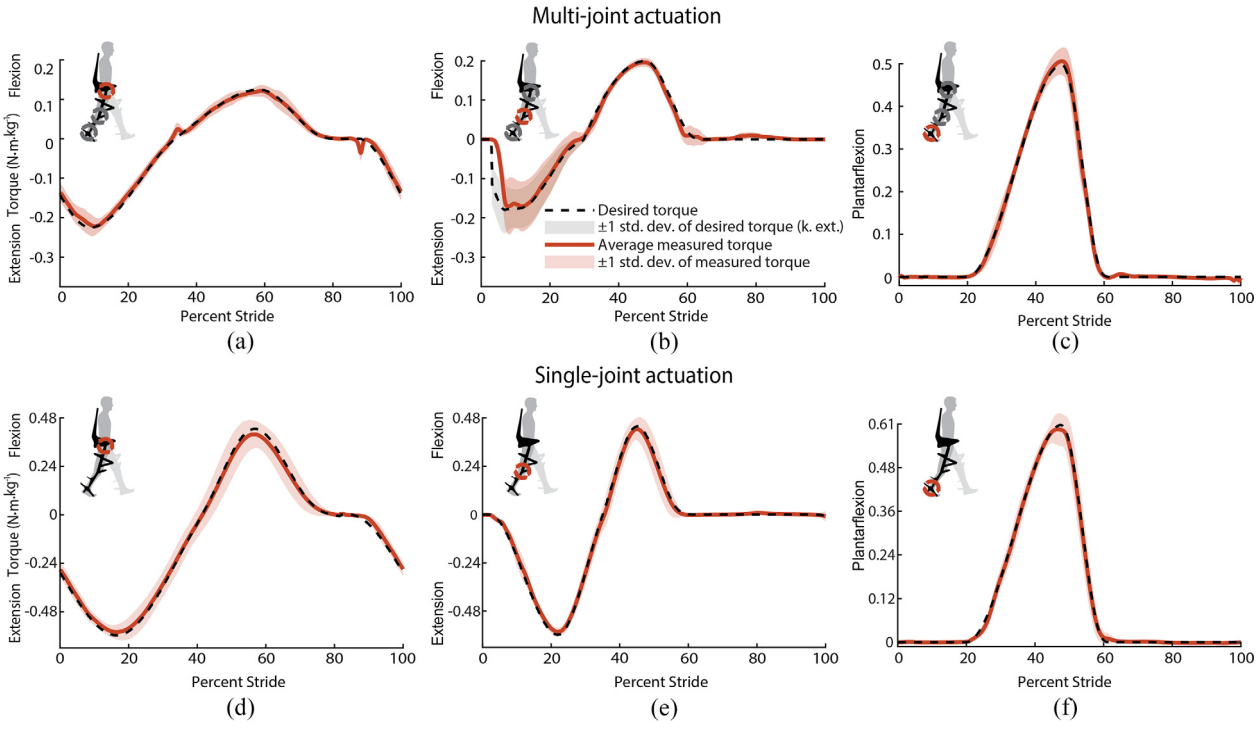

	Multi-joint actuation		Single-joint actuation	
	Total RMS error (N ·m)	Systematic RMS error (N ·m)	Total RMS error (N ·m)	Systematic RMS error (N ·m)
Hips	1.28	0.45	3.40	1.83
Knees	2.68	2.11	3.73	1.39
Ankles	1.47	0.19	2.25	1.02
Average	1.81	0.91	3.13	1.41

(g)

Fig. 22. Multi-joint and single-joint torque tracking during walking. (a) Hip, (b) knee, and (c) ankle torque tracking during multi-joint actuation. Desired torque (black, dashed), average measured torque (red), and ±1 standard deviation of measured torque (light red) are shown for each profile averaged over percent stride. All joints were evaluated simultaneously with peak torques up to 0.5 Nm/kg. Measured torques were recorded over 3 min and averaged across five participants. For knee extension during multi-joint actuation (b), desired torque is commanded by a virtual spring based on knee joint angle during stance. The ±1 standard deviation of desired knee extension torque (gray) shows how the desired torque varies between strides as knee angle varies. (d) Hip, (e) knee, and (f) ankle torque tracking during single-joint actuation for one experienced 86 kg user. Torque was applied to each joint individually with a peak torque of 0.61 Nm/kg. This test demonstrates the device's ability to track large torques during walking. (g) Table of torque tracking error. RMS error was calculated both over the entire trial (total RMS error) and as the error between the average measured torque per stride and the desired torque trajectory (systematic RMS error) for both multi-joint and single-joint actuation.

walked on a 15° incline at 0.75 m/s, walked at 1.25 m/s with a 11.5 kg load, and ran at 2.68 m/s. Movies of walking with and without torques, walking in various conditions with torques, and running with torques are included as Multimedia extensions 1 and 2.

7. Discussion

This exoskeleton emulator has the highest torque capabilities of any exoskeleton to date. It is one of few torque-controlled devices that assists the hips, knees and ankles (Yan et al., 2015; Young and Ferris, 2017). It is the only hip–knee–ankle exoskeleton that is cable-driven, a strategy that has been effective for both tethered (Quinlivan et al., 2017; Zhang et al., 2017) and mobile devices (Lee et al., 2018). These characteristics enable the exploration of a wide range of assistance strategies for walking, running, and load carriage (Extension 2) and to potentially assist with higher torque and power activities such as sprinting and jumping (Browning et al., 2007; Ong et al., 2016).

7.1. Device comparison

The exoskeleton emulator has an exceptional combination of torque, estimated power, estimated velocity, and bandwidth. To contextualize the system's performance, we compared these capabilities, as well as its weight, specific power, and specific torque, with other performance-augmentation exoskeletons for each joint (Figure 23 and Table 3). Our device has the highest or second highest torque, estimated power, and estimated velocity capabilities at all joints. In addition, it has among the highest specific torque, specific power, and bandwidth capabilities of exoskeletons. Soft exosuits have the lowest mass and high specific torque, indicating that they could be a better approach in applications where low mass is critical and high torque is not needed. As previous multi-joint exoskeletons were either limited by worn mass (Zoss et al., 2005) or torque capabilities (Ding et al., 2018; Quinlivan et al., 2017), we expect our device to find effective assistance strategies that were impossible for previous devices.

7.2. Device design

The exoskeleton is lightweight considering its high torque capabilities. Because the exoskeleton utilizes off-board motors and power sources, the worn mass is lower than that of a comparable mobile system. The mass distribution of a device can be used to estimate the expected increase in metabolic cost during walking (Browning et al., 2007). Based on the mass distribution of our device, we estimate that it would increase the metabolic cost of walking by 1.21 W/kg. This is consistent with the increase of 1.18 ± 0.39 W/kg we found experimentally. The hip–knee–ankle exoskeleton with the next highest capabilities is 27 kg heavier than our device (Zoss et al., 2005). If we assume a mass distribution similar to our device (Table 1), BLEEX is expected to increase the metabolic cost by 3.66 W/kg.

The exoskeleton is sufficiently compliant and low profile for walking and running. Users reported low stiffness in hip adduction and abduction, but relatively high stiffness in hip internal and external rotation. The user would have to apply an additional 7.57 Nm in hip abduction and 7.13 Nm in hip rotation to achieve typical kinematics for walking without the exoskeleton, corresponding to 7° abduction and 7° of hip external rotation (Novacheck, 1998; Wren et al., 2008). For a 50th percentile US male (CDC, 2015), the device applies up to 11% of biological hip adduction and abduction torque (MacKinnon and Winter, 1993) and 55% of biological hip internal and external rotation torque (Segal et al., 2011). The device stiffness is expected to passively assist hip adduction and abduction instead of impede it; the torque produced by the exoskeleton flexure is in the same direction as moments produced by hip musculature. Users reported minimal impedance to spinal axial rotation and spinal lateral bending during walking. This is likely due to the low stiffness of the back strut and the compliance in the chest harness, which allow for relative motion between the user and the exoskeleton. Users found ankle inversion-eversion stiffness to be high, but this stiffness may not necessarily increase metabolic rate; even complete fixation of the ankle can result in only small changes to metabolic rate (Vanderpool et al., 2008). Special attention was placed on making the medial components of the leg segments low profile, with a resulting medial envelope that is similar to that of previous, effective ankle exoskeletons (Witte et al., 2015). However, leg-to-leg contacts do occur occasionally and could lead to increased circumduction. This increased circumduction could contribute to the increase in metabolic cost (Shorter et al., 2017).

An exoskeleton emulator that is too heavy or bulky could alter participant biomechanics so much that assistance approaches discovered with the device would no longer be relevant to more streamlined mobile systems. Based on the results of the compliance and metabolic impact tests, we do not expect to encounter this issue with our present system. Anecdotally, we have also observed the biomechanical impact of the device decrease with experience.

The pin joints of the exoskeleton are sufficient for interfacing with the complex biological hip, knee, and ankle joints. Pin joints inherently result in some misalignment between the biological and device joint centers, but the misalignment does not cause additional, unexpected torque about the joint. Previously, a knee exoskeleton with pin joints was found to be more comfortable and substantially lighter than an exoskeleton that attempted to mimic the moving axis of rotation of the biological knee (Witte et al., 2017). This differs from other approaches at the knee which have no joint at all (Park et al., 2020) or try to track the biological joint center (Choi et al., 2017; Lee et al., 2017c). Users reported no sagittal plane joint impedance when the exoskeleton was sized correctly, but did report impedance if the exoskeleton was substantially misaligned. This indicates that the resolution of adjustability and the self-aligning nature of the straps allow for sufficient alignment of biological and mechanical axes of rotation. While there is no explicit joint for hip adduction and abduction, future devices could incorporate an explicit joint and actuation in that direction. Such actuation could be helpful for walking assistance, especially under load (Dembia et al., 2017).

To ensure the exoskeleton is an effective tool for studying walking and running assistance, some design compromises were necessary. The device is adjustable to fit a wide range of participants. Including this adjustability incurs a mass penalty due to overlapping material that is not loaded for smaller participants, additional attachment hardware, and the associated limitations on geometries that could be more mass optimal. In addition, this device has high torque capabilities, making it heavier than what an exoskeleton emulator designed for lower torques could weigh. An exoskeleton emulator designed for low-torque applications could be beneficial for exploring assistance in clinical populations, or when emulating low-mass, low-torque devices. However, our device is still capable of applying these low torques and is lighter than many low-torque

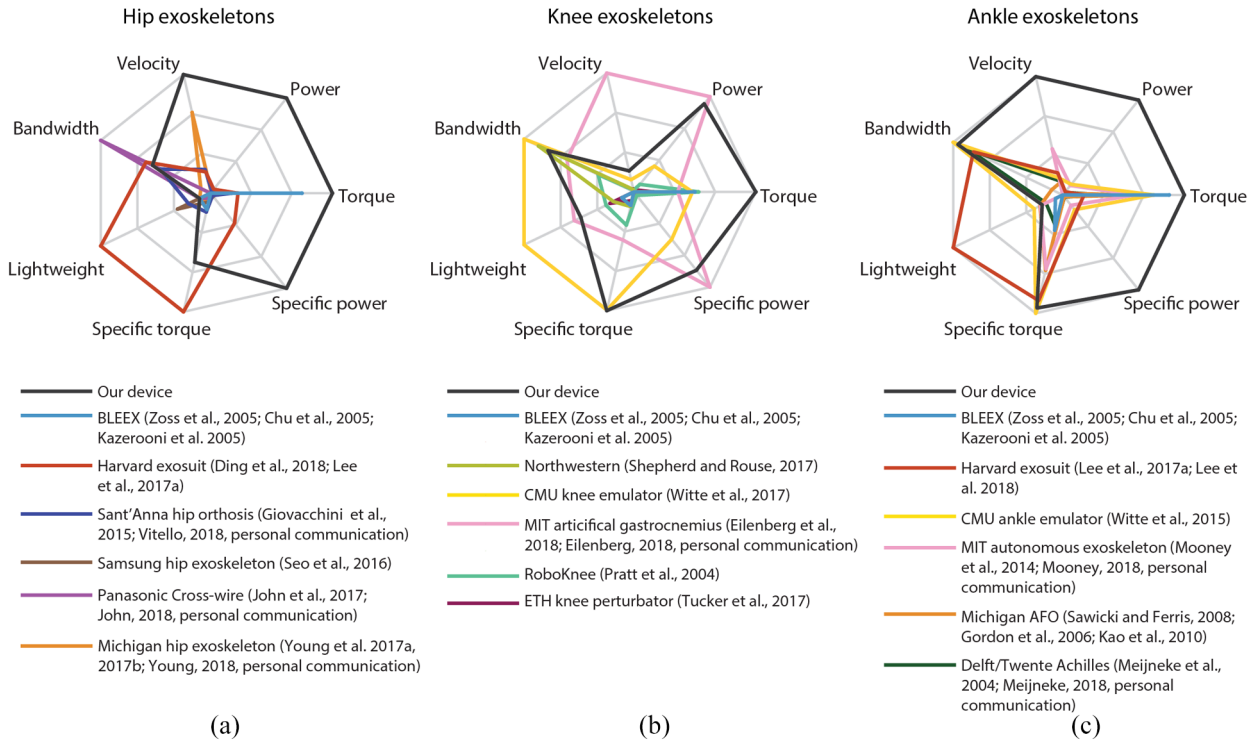

Fig. 23. Comparison of exoskeletons that assist the hip, knee, and ankle. (a) Exoskeletons that actuate the hip. (b) Exoskeletons that actuate the knee. (c) Exoskeletons that actuate the ankle. The data for this figure and any estimations made are found in Table 3. For each metric, the outermost point corresponds to the best value for the given trait, and each other point was normalized as a percentage of that value. For the torque-to-weight, power-to-weight, and lightweight metrics, estimated joint mass was used to allow for comparison between single-joint and multi-joint devices. The lightweight metric was calculated by taking the joint mass of the lightest exoskeleton and dividing it by the joint mass of each exoskeleton. Values that were not reported and could not be estimated were plotted as zero. Most of the included exoskeletons are designed for different applications, so direct comparison is not always relevant. This comparison is meant to contextualize the capabilities of our device and demonstrate its potential as an exoskeleton research tool.

mobile devices. Explicit degrees of freedom, with or without actuation, for internal–external hip rotation, hip adduction–abduction, and ankle inversion/eversion could be beneficial for studying loaded walking, balance or turning scenarios. However, the additional degrees of freedom would come with an additional weight penalty.

The system's off-board motors and control hardware preclude overground walking tests but provide great flexibility for laboratory-based experiments. In addition to walking on level ground, the system can emulate other real-world applications such as inclines (Extension 2), stair-climbing, rough terrain (Voloshina et al., 2013), and self-paced walking speeds (Sloot et al., 2014). Leveraging the laboratory environment makes it easier to capture kinematic, kinetic, and EMG data than working outside of the laboratory.

Although the laboratory environment makes it easier to capture biomechanical data, there are inherent challenges owing to the structure of the device. Many of the typical motion capture marker locations are occluded by the device, and reflective aluminum components result in ghost markers if not covered. Collecting EMG data is also made more difficult; the device structure and straps can impede placement of some sensors, donning and doffing can cause sensors to shift, torque application can be seen in EMG signals owing to motion artifacts, and the device causes additional electrical noise. Although many typical biomechanics data collection methods are more complicated with this system, we are in the process of developing new methods for collecting and analyzing essential biomechanics data.

7.3. Human subject tests

Wearing the device increases the metabolic cost of walking. For nine users, the increase in the metabolic cost of walking was 1.18 ± 0.39 W/kg on average. This corresponds to a metabolic increase of $38.9 \pm 12\%$ relative to walking without the device. To overcome that metabolic impact, exoskeleton assistance would need to provide a $27.5 \pm 6.3\%$ reduction relative to walking in the device unassisted. For the three experienced participants in this group, the device increased metabolic cost by 0.74 ± 0.07 W/kg, corresponding to a metabolic increase of $24.9 \pm 1.4\%$ relative to walking without the device. Exoskeleton assistance would need to provide a $19.9\% \pm 0.9\%$ reduction to overcome this

Table 3. Exoskeleton comparison table. Performance capabilities, including mass, are compared for a wide variety of exoskeletons. Values for the torque metrics are based on the highest applied torques (either on a test stand or on a person). Specific torque and specific power are calculated using estimated joint mass. Hip exoskeleton joint masses are bilateral, whereas knee and ankle devices are unilateral, because no unilateral hip exoskeletons were found.

Hip exoskeletons

	Our device	BLEEX[1-3]	Harvard[4,5]	Sant'Anna[6,7]	Samsung[8]	Panasonic[9,10]	Michigan[11-13]
Peak torque ($N \cdot m$)	200	150*	45†	35	11	20	23
Power (W)	4900‖	n. r.	203‡	80§	70‖	127§,‖	52*
Velocity ($rad \cdot s^{-1}$)	25‖	n. r.	4.5	5.0	n. r.	n. r.	17*
Bandwidth (Hz)	18	n. r.	20	16	n. r.	34	3.0§
Estimated Joint Mass (kg)	6.6¶	21**	0.86	4.2	2.8	9.3	6.8
Specific torque ($N \cdot m \cdot kg^{-1}$)	31	7*	52†	8	4	2	3
Specific power ($W \cdot kg^{-1}$)	748‖	n. r.	236‡	19§	25‖	14§,‖	8*
Total device mass (kg)	14	41	0.86	4.2	2.8	9.3	6.8
Mobile	No	Yes	Yes/No††	Yes	Yes	Yes	No

Knee exoskeletons

	Our device	BLEEX[1-3]	Northwestern[14]	Carnegie Mellon[15]	MIT[16,17]	Roboknee[18]	ETH Zurich[19]
Peak torque ($N \cdot m$)	250	125*	80	120	90	133	41
Power (W)	7400‖	n. r.	n. r.	2160‡,‖	8000§,‖	634	177
Velocity ($rad \cdot s^{-1}$)	31‖	n. r.	3.5	18‖	175§,‖	2.5	4.4
Bandwidth (Hz)	18	n. r.	20	23	14	7.5	n. r.
Estimated Joint Mass (kg)‡‡	1. 6¶	6.8**	4.1	0.76	1.4	3.0	3.5
Specific torque ($N \cdot m \cdot kg^{-1}$)	159	18*	20	158	64	44	12
Specific power ($W \cdot kg^{-1}$)	4698‖	n. r.	n. r.	2842‡,‖	5714§,‖	211	50
Total device mass (kg)	14	41	4.1	0.76	1.9	3.0	3.5
Mobile	No	Yes	Yes	No	No	Yes	No

Ankle exoskeletons

	Our device	BLEEX[1-3]	Harvard[5,20]	Carnegie Mellon[21]	MIT[22,23]	Michigan[24-26]	Achilles[27,28]
Peak torque ($N \cdot m$)	200	175*	40†	150	120	120	68§
Power (W)	7000‖	n. r.	268‡	780‡	700§,‖	123*	192
Velocity ($rad \cdot s^{-1}$)	36‖	n. r.	6.7	5.2	14§,‖	3.7*	4.3§
Bandwidth (Hz)	23	n. r.	20	24	n. r.	2.4	21
Estimated Joint Mass (kg)‡‡	1.2¶	3.4**	0.28§ §	0.88	1.1‖‖	1.1	1.5‖‖
Specific torque ($N \cdot m \cdot kg^{-1}$)	164	51*	145†	171	107	109	45§
Specific power ($W \cdot kg^{-1}$)	5738‖	n. r.	975‡	891‡	625§,‖	112*	128
Total device mass (kg)	14	41.0	1.1	0.88	4.0	1.1	8.2
Mobile	No	Yes	Yes/No††	No	Yes	No	Yes

n.r. Indicates data that was not reported and could not be estimated from reported data with reasonable accuracy. *Estimated from reported figures. †Calculated from reported cable forces and reported lever-arm estimates (Lee et al., 2017). ‡Estimated assuming that device strength is the torque-limiting factor (not actuator capabilities), such that the device can apply maximum torque near the maximum velocity, such that peak power can be approximated as $P_{max} = \tau_{max} \cdot \omega_{max}$. §Reported via personal communication with author. ‖Estimated from reported actuator capabilities. ¶Joint masses were calculated based on values from Table 1. For the hip, the joint mass was calculated as torso mass plus half of the thigh mass. For the knee, it was calculated as half of the thigh and shank masses. For the ankle it was calculated as the foot mass (sans boot) plus half of the shank mass. **Segment masses of BLEEX were estimated to be 1/2 of the system mass at the hip, 1/3 at the knee, and 1/6 at the ankle. ††Harvard exosuit exists both in mobile and tethered versions. Data from tethered versions was used for the best comparison. ‡‡Joint masses from bilateral devices were divided by two. For the ankle, the mass of any shoe or boot was ignored, since some exoskeletons did not report the weight of the shoe or boot. § §Ankle mass is estimated to be half of the total mass of the hip-ankle exosuit. ‖‖Joint mass excludes battery packs and control hardware that are placed at the waist. **1**. Zoss et al., 2005. **2**. Chu et al., 2005. **3**. Kazerooni et al., 2005. **4**. Ding et al., 2018. **5**. Lee et al., 2017. **6**. Giovacchini et al., 2015. **7**. Vitello, 2018, personal communication. **8**. Seo et al., 2016. **9**. John et al., 2017. **10.** John, 2018, personal communication. **11**. Young et al., 2017a. **12**. Young et al., 2017b. **13.** Young, 2018, personal communication. **14**. Shepherd and Rouse, 2017. **15**. Witte et al., 2017. **16**. Eilenberg et al., 2018. **17.** Eilenberg, 2018, personal communication. **18**. Pratt et al., 2004. **19**. Tucker et al., 2017. **20**. Lee et al. 2017a. **21**. Witte et al. 2015. **22**. Mooney et al., 2014. **23**. Mooney, 2018, personal communication. **24**. Sawicki and Ferris, 2008. **25**. Gordon et al., 2006. **26**. Kao et al., 2010. **27**. Meijneke et al., 2014. **28**. Meijneke, 2018, personal communication.

impact. This suggests that while the penalty for naive participants is relatively high, this penalty may decrease with experience in the device. In a separate study (Jackson and Collins, 2019) with bilateral ankle exoskeletons, the reduction needed to offset the device was 13.8%. Given the increase in number of actuated joints and magnitude of available torque, a required reduction of 27.5% seems reasonable. We expect a net reduction in effort when the device applies effective assistance strategies.

Users generally found the exoskeleton comfortable, rating it on average 5 out of 7 after 30 min of walking in the device. Another indicator of device comfort is if users can walk with applied torques for long sessions and over multiple days. Three users have walked for 3 h in a single session and one user has walked for 14 h over multiple sessions in 1 month. For the five users who completed the comfort evaluation, all users indicated that the primary source of discomfort was the boots. This is likely because of the stiff construction of the boot and the limited number of sizes to fit all users. A redesigned foot segment with different boots may be able to improve user comfort. Most users could not feel the toe and heel rods in the boots. Foam padding on the medial knee and lateral hip components allow us to comfortably fit the exoskeleton to users with different leg geometries. Users also wear leggings to prevent any contact with their skin. Some users reported difficulty in arm swing owing to the location of the waist struts, which extend anteroposteriorly to enable attachment of the waist straps and full range of motion of the hips. Between users, differences in obstruction were likely related to the relative widths of users' hips and shoulders. In addition, one user who ran in the device noted increased arm swing was necessary (Extension 2), likely due to the added distal mass (Collins et al., 2009).

Applied forces were sufficiently comfortable. For five novice users, there was no significant change in the average overall comfort rating between walking without torques (Figure 21(b), 15 min.) and walking with torques (Figure 21(b), 30 min.) (two-tailed paired t-test, $p = 0.62$). Straps were placed on bony landmarks and muscles, locations that we have found to be most comfortable for applying forces to the user's body. For each segment, straps are located far from each other to reduce the applied force on the user. Straps located high on the torso are intended to assist the core muscles that are typically active during biological hip torques (Winter, 1991). In addition, the timing of torques can have an effect on comfort. The force applied to the torso can be reduced if hip flexion and extension torques are applied to opposite legs simultaneously, resulting in a smaller net force (Figure 10(a) and (b)). This occurs for biological torques during normal walking and running.

7.4. Torque application

The exoskeleton accurately applied torques during walking. For five users with multi-joint torques and one user with large single-joint torques applied, the RMS errors of torque tracking are within 0.5 Nm of errors reported by other devices for similar torque magnitudes (Shepherd and Rouse, 2017; Witte et al., 2017). As optimal torque profiles are found for walking and running, we expect the optimized magnitudes will approach these larger tested magnitudes, while remaining within device capabilities. The relatively low torque magnitudes tested during multi-joint actuation were to ensure that novice users could walk easily. Highly variable friction in the Bowden cable transmission was likely a major source of tracking error. Another source of error could be from the variable knee extension torque profile (Figure 22(b)). The profile has discontinuities at the onset and offset of the desired torque, and iterative learning is unable to compensate for stride-to-stride changes, leading to larger RMS error compared with the hips and ankles.

8. Conclusion

The strategies found using this exoskeleton emulator will improve human mobility and inform the design of new exoskeletons. By using human-in-the-loop optimization, new assistance strategies can be found for walking and running at various speeds, grades, and loads. Higher torque applications could also be explored, such as sprinting and jumping. We can use this understanding of optimal assistance of the entire lower limb to emulate new viable exoskeleton designs, accelerate research in the field, enable the development of new products, and investigate new rehabilitation techniques in clinical settings. The technologies that this research enables could have a transformative effect on the productivity, health, and quality of life of workers, first responders, soldiers, older adults, and people with disabilities.

Acknowledgments

We would like to thank K. Gregorczyk, G. Kanagaki, M. O'Donovan, and the NSRDEC for their input on system design and characteristics and their assistance with the design of the comfort experiments, K. Witte, V. Chiu, K. Poggensee, and J. Caputo for feedback on design and data collection, K. Wang for assistance in design and manufacturing, N. Bianco for assistance in controller development, R. Jackson for editorial suggestions, and M. Eilenberg, S. John, C. Meijneke, L. Mooney, G. Sawicki, M. Shepherd, C. Shirota, N. Vitiello, A. Young, and A. Zoss for information on device capabilities.

Funding

This work was supported by the U.S. Army Natick Soldier Research, Development, and Engineering Center (grant number W911QY18C0140).

References

Awad LN, Bae J, O'Donnell K, et al. (2017) A soft robotic exosuit improves walking in patients after stroke. *Science Translational Medicine* 9(400): eaai9084.

Bach Baunsgaard, C Vig Nissen U, Katrin Brust A, et al. (2018) Gait training after spinal cord injury: safety, feasibility and gait function following 8 weeks of training with the exoskeletons from Ekso Bionics. *Spinal Cord* 56(2): 106–116.

Browning RC, Modica JR, Kram R and Goswami A (2007) The effects of adding mass to the legs on the energetics and biomechanics of walking. *Medicine and Science in Sports and Exercise* 39(3): 515–525.

Caputo JM, Adamczyk PG and Collins SH (2015) Informing ankle–foot prosthesis prescription through haptic emulation of candidate devices. In: *2015 IEEE International Conference on Robotics and Automation (ICRA)*, pp. 6445–6450.

Caputo JM and Collins SH (2014) A universal ankle–foot prosthesis emulator for human locomotion experiments. *Journal of Biomechanical Engineering* 136(3): 035002.

CDC (2015) National Health and Nutrition Examination Survey. *Technical report, National Center for Health Statistics, Centers for Disease Control and Prevention*. Available at: https://wwwn.cdc.gov/nchs/nhanes/continuousnhanes/default.aspx?-BeginYear=2015 (accessed September 2020).

Choi B, Lee Y, Kim YJ, et al. (2017) Development of adjustable knee joint for walking assistance devices. In: *2017 IEEE/RSJ International Conference on Intelligent Robots and Systems (IROS)*, pp. 1790–1797.

Chu A, Kazerooni H and Zoss A (2005) On the biomimetic design of the Berkeley Lower Extremity Exoskeleton (BLEEX). In: *Proceedings of the 2005 IEEE International Conference on Robotics and Automation (ICRA)*, Barcelona, Spain, pp. 4345–4352.

Collins SH, Adamczyk PG and Kuo AD (2009) Dynamic arm swinging in human walking. *Proceedings of the Royal Society B: Biological Sciences* 276(1673): 3679–3688.

Collins SH, Wiggin MB and Sawicki GS (2015) Reducing the energy cost of human walking using an unpowered exoskeleton. *Nature* 522(7555): 212–215.

Corlett EN and Bishop RP (1976) A technique for assessing postural discomfort. *Ergonomics* 19(2): 175–182.

Dembia CL, Silder A, Uchida TK, Hicks JL and Delp SL (2017) Simulating ideal assistive devices to reduce the metabolic cost of walking with heavy loads. *PLoS ONE* 12(7): e0180320.

Ding Y, Galiana I, Asbeck A, Quinlivan B, Rossi SMMD and Walsh C (2014) Multi-joint actuation platform for lower extremity soft exosuits. In: *2014 IEEE International Conference on Robotics and Automation (ICRA)*, pp. 1327–1334.

Ding Y, Galiana I, Asbeck AT, et al. (2017) Biomechanical and physiological evaluation of multi-joint assistance with soft exosuits. *IEEE Transactions on Neural Systems and Rehabilitation Engineering* 25(2): 119–130.

Ding Y, Kim M, Kuindersma S and Walsh CJ (2018) Human-in-the-loop optimization of hip assistance with a soft exosuit during walking. *Science Robotics* 3(15): eaar5438.

Ding Y, Panizzolo FA, Siviy C, et al. (2016) Effect of timing of hip extension assistance during loaded walking with a soft exosuit. *Journal of NeuroEngineering and Rehabilitation* 13(1): 87.

Eilenberg MF, Kuan JY and Herr H (2018) Development and evaluation of a powered artificial gastrocnemius for transtibial amputee gait. *Hindawi Journal of Robotics* 2018: 5951965.

Esquenazi A, Talaty M, Packel A and Saulino M (2012) The ReWalk powered exoskeleton to restore ambulatory function to individuals with thoracic-level motor-complete spinal cord injury. *American Journal of Physical Medicine and Rehabilitation* 91(11): 911–921.

Farris RJ, Quintero HA and Goldfarb M (2011) Preliminary evaluation of a powered lower limb orthosis to aid walking in paraplegic individuals. *IEEE Transactions on Neural Systems and Rehabilitation Engineering* 19(6): 652–659.

Felt W, Selinger JC, Donelan JM and Remy CD (2015) 'Body-In-The-Loop': optimizing device parameters using measures of instantaneous energetic cost. *PLoS ONE* 10(8): e0135342.

Giovacchini F, Vannetti F, Fantozzi M, et al. (2015) A light-weight active orthosis for hip movement assistance. *Robotics and Autonomous Systems* 73: 123–134.

Gordon KE, Sawicki GS and Ferris DP (2006) Mechanical performance of artificial pneumatic muscles to power an ankle–foot orthosis. *Journal of Biomechanics* 39(10): 1832–1841.

Griffin R, Cobb T, Craig T, et al. (2017) Stepping forward with exoskeletons: Team IHMC's design and approach in the 2016 Cybathlon. *IEEE Robotics and Automation Magazine* 24(4): 66–74.

Griffiths PG, Gillespie RB and Freudenberg JS (2011) A fundamental linear systems conflict between performance and passivity in haptic rendering. *IEEE Transactions on Robotics* 27(1): 75–88.

Jackson RW and Collins SH (2019) Heuristic-based ankle exoskeleton control for co-adaptive assistance of human locomotion. *IEEE Transactions on Neural Systems and Rehabilitation Engineering* 27(10): 2059–2069.

Jezernik S, Colombo G, Keller T, Frueh H and Morari M (2003) Robotic orthosis lokomat: A rehabilitation and research tool. *Neuromodulation* 6(2): 108–115.

Jin X, Cui X and Agrawal SK (2015) Design of a cable-driven active leg exoskeleton (C-ALEX) and gait training experiments with human subjects. In: *2015 IEEE International Conference on Robotics and Automation (ICRA)*, pp. 5578–5583.

John SW, Murakami K, Komatsu M and Adachi S (2017) Crosswire assist suit concept, for mobile and lightweight multiple degree of freedom hip assistance. In: *2017 IEEE International Conference on Rehabilitation Robotics (ICORR)*, pp. 387–393.

Kao PC, Lewis CL and Ferris DP (2010) Invariant ankle moment patterns when walking with and without a robotic ankle exoskeleton. *Journal of Biomechanics* 43(2): 203–209.

Kazerooni H, Racine JL and Huang L (2005) On the control of the Berkeley Lower Extremity Exoskeleton (BLEEX). In: *Proceedings of the 2005 IEEE International Conference on Robotics and Automation (ICRA)*, Barcelona, Spain, pp. 4353–4360.

Kilicarslan A, Prasad S, Grossman RG and Contreras-Vidal JL (2013) High accuracy decoding of user intentions using EEG to control a lower-body exoskeleton. In: *International Conference of the IEEE Engineering in Medicine and Biology Society*, (EMBC), pp. 5606–5609.

Kim J, Lee G, Heimgartner R, et al. (2019) Reducing the metabolic rate of walking and running with a versatile, portable exosuit. *Science* 365(6454): 668–672.

Kim M, Ding Y, Malcolm P, Kim M, Ding Y, Malcolm P, Speeckaert J, Siviy C.J, Walsh C.J. and Kuindersma S. (2017) Human-in-the-loop Bayesian optimization of wearable device parameters. PLoS ONE 12(9): e0184054.

Koller JR, Gates DH, Ferris DP and Remy CD (2016) 'Body-in-the-Loop' optimization of assistive robotic devices: A validation study. In: *Robotics: Science and Systems*.

Lee G, Ding Y, Bujanda IG, Karavas N, Zhou YM and Walsh CJ (2017a) Improved assistive profile tracking of soft exosuits for walking and jogging with off-board actuation. In: *2017 IEEE/*

RSJ International Conference on Intelligent Robots and Systems (IROS), pp. 1699–1706.

Lee G, Kim J, Panizzolo FA, et al. (2017b) Reducing the metabolic cost of running with a tethered soft exosuit. *Science Robotics* 2(6): eaan6708.

Lee S, Kim J, Baker L, et al. (2018) Autonomous multi-joint soft exosuit with augmentation-power-based control parameter tuning reduces energy cost of loaded walking. *Journal of NeuroEngineering and Rehabilitation* 15(1): 66.

Lee Y, Kim YJ, Lee J, et al. (2017c) Biomechanical design of a novel flexible exoskeleton for lower extremities. *IEEE/ASME Transactions on Mechatronics* 22(5): 2058–2069.

MacKinnon CD and Winter DA (1993) Control of whole body balance in the frontal plane during human walking. *Journal of Biomechanics* 26(6): 633–644.

Maeshima S, Osawa A, Nishio D, et al. (2011) Efficacy of a hybrid assistive limb in post-stroke hemiplegic patients: A preliminary report. *BMC Neurology* 11 (1): 116.

Malcolm P, Derave W, Galle S and De Clercq D (2013) A simple exoskeleton that assists plantarflexion can reduce the metabolic cost of human walking. *PLoS ONE* 8(2): e56137.

Malcolm P, Galle S, Derave W and De Clercq D (2018a) Bi-articular knee-ankle-foot exoskeleton produces higher metabolic cost reduction than weight-matched mono-articular exoskeleton. *Frontiers in Neuroscience* 12: 00069.

Malcolm P, Galle S, Van den Berghe P and De Clercq D (2018b) Exoskeleton assistance symmetry matters: Unilateral assistance reduces metabolic cost, but relatively less than bilateral assistance. *Journal of NeuroEngineering and Rehabilitation* 15(1): 74.

Meijneke C, van Dijk W and van der Kooij H (2014) Achilles: An autonomous lightweight ankle exoskeleton to provide push-off power. In: *5th IEEE RAS/EMBS International Conference on Biomedical Robotics and Biomechatronics*, pp. 918–923.

Mooney LM, Rouse EJ and Herr HM (2014) Autonomous exoskeleton reduces metabolic cost of human walking during load carriage. *Journal of NeuroEngineering and Rehabilitation* 11(1): 80.

Nasiri R, Ahmadi A and Ahmadabadi MN (2018) Reducing the energy cost of human running using an unpowered exoskeleton. *IEEE Transactions on Neural Systems and Rehabilitation Engineering* 26: 2026–2032.

Novacheck TF (1998) The biomechanics of running. *Gait and Posture* 7(1): 77–95.

Ong CF, Hicks JL and Delp SL (2016) Simulation-based design for wearable robotic systems: An optimization framework for enhancing a standing long jump. *IEEE Transactions on Biomedical Engineering* 63(5): 894–903.

Park EJ, Akbas T, Eckert-Erdheim A, et al. (2020) A hinge-free, non-restrictive, lightweight tethered exosuit for knee extension assistance during walking. *IEEE Transactions on Medical Robotics and Bionics* 2(2): 165–175.

Pratt JE, Krupp BT, Morse CJ and Collins SH (2004) The RoboKnee: An exoskeleton for enhancing strength and endurance during walking. In: *2004 IEEE International Conference on Robotics and Automation (ICRA)*, Vol. 3, pp. 2430–2435.

Quinlivan BT, Lee S, Malcolm P, et al. (2017) Assistance magnitude versus metabolic cost reductions for a tethered multiarticular soft exosuit. *Science Robotics* 2(2): eaah4416.

Roberts TJ and Belliveau RA (2005) Sources of mechanical power for uphill running in humans. *The Journal of Experimental Biology* 208(10): 1963–1970.

Sawicki GS, Beck ON, Kang I and Young AJ (2020) The exoskeleton expansion: Improving walking and running economy. *Journal of NeuroEngineering and Rehabilitation* 17(1): 1–9.

Sawicki GS and Ferris DP (2008) Mechanics and energetics of level walking with powered ankle exoskeletons. *Journal of Experimental Biology* 211(9): 1402–1413.

Segal AD, Orendurff MS, Czerniecki JM, Schoen J and Klute GK (2011) Comparison of transtibial amputee and non-amputee biomechanics during a common turning task. *Gait and Posture* 33(1): 41–47.

Seo K, Lee J, Lee Y, Ha T and Shim Y (2016) Fully autonomous hip exoskeleton saves metabolic cost of walking. In: *2016 IEEE International Conference on Robotics and Automation (ICRA)*, pp. 4628–4635.

Shepherd MK and Rouse EJ (2017) Design and validation of a torque-controllable knee exoskeleton for sit-to-stand assistance. *IEEE/ASME Transactions on Mechatronics* 22(4): 1695–1704.

Shorter KA, Wu A and Kuo AD (2017) The high cost of swing leg circumduction during human walking. *Gait and Posture* 54: 265–270.

Simpson CS, Welker CG, Uhlrich SD, et al. (2019) Connecting the legs with a spring improves human running economy. *Journal of Experimental Biology* 222(17): jeb202895.

Sloot LH, van der Krogt MM and Harlaar J (2014) Self-paced versus fixed speed treadmill walking. *Gait and Posture* 39(1): 478–484.

Tucker MR, Shirota C, Lambercy O, Sulzer JS and Gassert R (2017) Design and characterization of an exoskeleton for perturbing the knee during gait. *IEEE Transactions on Biomedical Engineering* 64(10): 2331–2343.

Uchida TK, Seth A, Pouya S, Dembia CL, Hicks JL and Delp SL (2016) Simulating ideal assistive devices to reduce the metabolic cost of running. *PLoS ONE* 11(9): e0163417.

Vanderpool MT, Collins SH and Kuo AD (2008) Ankle fixation need not increase the energetic cost of human walking. *Gait and Posture* 28(3): 427–433.

Voloshina AS, Kuo AD, Daley MA and Ferris DP (2013) Biomechanics and energetics of walking on uneven terrain. *Journal of Experimental Biology* 216(21): 3963–3970.

Wang S, Wang L, Meijneke C, et al. (2015) Design and control of the MINDWALKER exoskeleton. *IEEE Transactions on Neural Systems and Rehabilitation Engineering* 23(2): 277–286.

Winter DA (1991) *The Biomechanics and Motor Control of Human Gait: Normal, Elderly and Pathological*. 2nd edn. Waterloo Biomechanics.

Witte KA, Fatschel AM and Collins SH (2017) Design of a lightweight, tethered, torque-controlled knee exoskeleton. In: *2017 International Conference on Rehabilitation Robotics (ICORR)*, pp. 1646–1653.

Witte K. A, Fiers P, Sheets-Singer A. L and Collins S. H. (2020) Improving the energy economy of human running with powered and unpowered ankle exoskeleton assistance. Science Robotics, 5:eaay9108.

Witte KA, Zhang J, Jackson RW and Collins SH (2015) Design of two lightweight, high-bandwidth torque-controlled ankle exoskeletons. In: *2015 IEEE International Conference on Robotics and Automation (ICRA)*, pp. 1223–1228.

Wren TA, Do KP, Hara R and Rethlefsen SA (2008) Use of a patella marker to improve tracking of dynamic hip rotation range of motion. *Gait and Posture* 27(3): 530–534.

Yan T, Cempini M, Oddo CM and Vitiello N (2015) Review of assistive strategies in powered lower-limb orthoses and exoskeletons. *Robotics and Autonomous Systems* 64: 120–136.

Young AJ and Ferris DP (2017) State of the art and future directions for lower limb robotic exoskeletons. *IEEE Transactions on Neural Systems and Rehabilitation Engineering* 25(2): 171–182.

Young AJ, Foss J, Gannon H and Ferris DP (2017a) Influence of power delivery timing on the energetics and biomechanics of humans wearing a hip exoskeleton. *Frontiers in Bioengineering and Biotechnology* 5: 00004.

Young AJ, Gannon H and Ferris DP (2017b) A biomechanical comparison of proportional electromyography control to biological torque control using a powered hip exoskeleton. *Frontiers in Bioengineering and Biotechnology* 5: 00037.

Zhang J, Cheah CC and Collins SH (2015) Experimental comparison of torque control methods on an ankle exoskeleton during human walking. In: *2015 IEEE International Conference on Robotics and Automation (ICRA)*, pp. 5584–5589.

Zhang J, Fiers P, Witte KA, et al. (2017) Human-in-the-loop optimization of exoskeleton assistance during walking. *Science* 356(6344): 1280–1284.

Zoss A, Kazerooni H and Chu A (2005) On the mechanical design of the Berkeley Lower Extremity Exoskeleton (BLEEX). In: *2005 IEEE/RSJ International Conference on Intelligent Robots and Systems*, pp. 3465–3472.

Appendix. Index to multimedia extensions

Archives of IJRR multimedia extensions published prior to 2014 can be found at http://www.ijrr.org, after 2014 all videos are available on the IJRR YouTube channel at http://www.youtube.com/user/ijrrmultimedia

Table of Multimedia Extensions

1	Video	Walking with and without torque
2	Video	Hip–knee-ankle torques, speeds, grade and loads
3	Data	CAD models
4	Data	Bill of materials
5	Video	Benchtop tests
6	Video	Adjustability, donning, and doffing the exoskeleton
7	Data	RPSD questionnaire